nature plants

Article

https://doi.org/10.1038/s41477-025-01915-z

MADS31 supports female germline development by repressing the post-fertilization programme in cereal ovules

Received: 27 March 2023

Accepted: 13 January 2025

Published online: 25 February 2025

Check for updates

A list of authors and their affiliations appears at the end of the paper

The female germline of flowering plants develops within a niche of sporophytic (somatic) ovule cells, also referred to as the nucellus. How niche cells maintain their own somatic developmental programme, yet support the development of adjoining germline cells, remains largely unknown. Here we report that MADS31, a conserved MADS-box transcription factor from the B-sister subclass, is a potent regulator of niche cell identity. In barley, MADS31 is preferentially expressed in nucellar cells directly adjoining the germline, and loss-of-function *mads31* mutants exhibit deformed and disorganized nucellar cells, leading to impaired germline development and partial female sterility. Remarkably similar phenotypes are observed in *mads31* mutants in wheat, suggesting functional conservation within the Triticeae tribe. Molecular assays indicate that MADS31 encodes a potent transcriptional repressor, targeting genes in the ovule that are normally active in the seed. One prominent target of MADS31 is *NRPD4b*, a seed-expressed component of RNA polymerase IV/V that is involved in epigenetic regulation. *NRPD4b* is directly repressed by MADS31 in vivo and is derepressed in *mads31* ovules, while overexpression of *NRPD4b* recapitulates the *mads31* ovule phenotype. Thus, repression of *NRPD4b* by MADS31 is required to maintain ovule niche functionality. Our findings reveal a new mechanism by which somatic ovule tissues maintain their identity and support germline development before transitioning to the post-fertilization programme.

In seed-bearing plants, ovules are a complex mixture of diploid sporophytic (somatic) and haploid gametophytic tissues that perform distinct roles during reproduction. The most prominent somatic tissues include a distal nucellus, which gives rise to the female germline and gametophyte (embryo sac); the central chalaza, which gives rise to the protective integuments and seed coat; and the proximal funiculus, which connects the ovule to a supply of maternal nutrients[1]. Coordinated transitions between growth and differentiation in the ovule provide the scaffold for downstream seed development. For example, during early stages of ovule growth, the nucellus initiates a generative phase in which the germline is established within a pool of somatic cells[2]. Specifically, a single nucellus cell initiates megasporogenesis and differentiates into a megaspore mother cell (MMC). In most angiosperms, this cell divides by meiosis to give rise to four haploid megaspores, one of which undergoes three rounds of mitosis to form a single embryo sac, which contains an egg cell, two synergid cells, a central cell and multiple antipodal cells[3]. As the ovule matures, the integuments form a protective coat around the embryo sac, and the nucellus

e-mail: matthew.tucker@adelaide.edu.au

remodels to enter a nursing phase, showing signs of collapse, cell death and differentiation, in preparation for fertilization and seed initiation.

Also referred to as the megasporangium, the nucellus supports germline development from initiation until fertilization[1,4]. This role appears to be independent of the number of cells within the nucellus, which varies from relatively few cells in dicotyledonous *Arabidopsis*, to many in monocotyledonous cereals such as rice, barley and wheat[2,5]. Genetic studies indicate that the nucellus integrates multiple regulatory pathways to support the germline, many of which are not expressed in the germline itself[6]. Defects during the generative phase range in severity from subtle to extreme. For example, *Arabidopsis nozzle/sporocyteless* (*spl*) mutants produce a nucellus-like tissue but fail to initiate a germline[7,8], while maize *dmt103* DNA methyltransferase mutants show overproliferation of the nucellus and multiple embryo sacs[9]. Mutations in the *Arabidopsis RNA DEPENDENT RNA POLYMERASE6* (*RDR6*) and *ARGONAUTE9* (*AGO9*) small interfering RNA (siRNA) processing genes, or the rice *MSP1* leucine-rich receptor kinase-encoding gene, result in multiple nucellar cells adopting features of germline cells[10,11]. Moreover, inactivation of the *ARABIDOPSIS HISTIDINE KINASE* (*AHK*) cytokinin receptors[12], weak *pin-formed1* (*pin1*) mutants[13], or null *rab geranylgeranyl transferase beta subunit* (*rgtb1*) mutants where PIN1 function is compromised, produce a functional megaspore that fails to initiate gametogenesis[14]. The spatiotemporal coordination of these diverse pathways has remained unclear, although recent progress suggests that the D-class MADS-box gene *SEEDSTICK* (*STK*) acts upstream of epigenetic pathways in the nucellus to spatially regulate *SPL* expression, which in turn promotes auxin signalling and germline development[15].

During later stages of ovule and embryo sac development, the nucellus exhibits features characteristic of cell degeneration. In *Arabidopsis*, this process is regulated by auxin signalling and occurs concomitant with rapid expansion of the embryo sac[16]. In cereal species, nucellar degeneration is most obvious after fertilization and involves a range of programmed cell death-related elicitors including the novel Jekyll protein[17] and vacuolar processing enzyme 2a (VPE2a)[18]. Nucellar degeneration coincides with the establishment of transfer tissues that provide maternally derived nutrition to the endosperm[19,20]. For example, in rice, barley and wheat, the last vestige of the nucellus forms a transfer tissue referred to as the nucellar projection[21–23]. Taken together, these studies highlight how the nucellus influences multiple stages of sexual reproduction; despite this, the transcriptional drivers of nucellus maintenance, degeneration and differentiation remain largely unknown.

Along with *STK*, the plant-specific type II MIKC C-, D- and E-class MADS-box genes control ovule initiation[24] as well as tissue differentiation during ovule and seed development in *Arabidopsis*[25,26]. The subclass B-sister (Bsis) MADS-box proteins, also from the type II MIKC family, are mainly expressed in female reproductive organs[27,28]. The *Arabidopsis* genome contains two Bsis genes, *TRANSPARENT TESTA16/ARABIDOPSIS BSISTER* (*ABS*) and *GORDITA* (*GOA*)/*AGL63*. *ABS* promotes nucellus degradation[29], specifies the endothelium via interaction with *STK*[30], and influences deposition of pigments in the maturing integuments and seed coat[31]. *GOA*, a paralogue of *ABS*, is more widely expressed in ovules, seeds and fruits, contributing to fruit growth and integument/seed coat development[32,33]. However, neither *abs* nor *goa* show significant levels of ovule abortion, indicating their dispensable roles in determining fertility. In orchid, Bsis *PeMADS28* is expressed in the nucellus and integuments, and can rescue the *Arabidopsis abs* mutant[34]. In cereals, among three subclades of Bsis (MADS29, MADS30 and MADS31)[35], MADS29 is vital to seed formation. The *MADS29* gene is expressed in the nucellus and residual nucellar projection during seed development, and loss-of-function mutations in rice, barley and wheat cause seed abortion because of severely inhibited endosperm development[21–23,35,36]. Rice MADS30 regulates plant architecture and is not involved in female reproduction, a likely product of evolutionary neofunctionalization[37]. A role for the third member of the Bsis family in cereals, MADS31, has yet to be elucidated.

Here we show that MADS31 is preferentially expressed in the barley nucellus where it functions to maintain both nucellus identity and female germline development. MADS31 affects this function through the transcriptional repression of key genes involved in post-fertilization development, including epigenetic regulatory components and cell death pathways. Removal of MADS31 leads to precocious initiation of cell death, upregulation of seed development genes and altered cell morphology in the inner nucellus. Importantly, similar ovule phenotypes are observed in a *Tamads31* mutant of *Triticum aestivum* (bread wheat), suggesting functional conservation between two Triticeae species. Therefore, MADS31 maintains the integrity of the cereal ovule until developmental constraints are released by fertilization. Our findings provide new insight regarding the maintenance of somatic ovule cells and their role in coordinating multiple stages of seed development.

Results

MADS31 is preferentially expressed in the inner nucellus

Previously, we established a tissue-specific transcriptome dataset for the barley ovule[38,39]. Cells were collected from the nucellus, integuments, ovary wall and embryo sac at different stages of ovule development before RNA was extracted and sequenced (Extended Data Fig. 1a). Genes that were preferentially expressed in the nucellus across multiple stages, rather than a single stage, were selected as candidate tissue-specific regulators (Supplementary Dataset 1; examples are shown in Extended Data Fig. 2). One of these, the Bsis class MADS-box gene *MADS31* (HORVU2Hr1G098930) showed abundant expression in the nucellus and lower expression in the integuments and embryo sac (Extended Data Fig. 1b). Notably, *MADS31* was the most abundant Bsis in the ovule relative to its paralogues *MADS29* and *MADS30* (Extended Data Fig. 2). Reverse transcription-quantitative polymerase chain reaction (RT–qPCR) showed that *MADS31* was specifically expressed in the pistil and was absent in vegetative tissues or other floral organs that were examined in this study (Fig. 1a). In the pistil, *MADS31* transcripts increased as the ovule developed from a primordium (Ov1) to mature female gametophyte stage (Ov9a), then decreased at anthesis (Ov9b and Ov10; Fig. 1b)[40]. We examined tissue specificity of the *MADS31* transcript and protein using messenger (m)RNA in situ hybridization and a transgenic line expressing a translational fusion of MADS31 to enhanced green fluorescent protein (eGFP) under the control of its native promoter (*pMADS31*). At Ov2 stage, when the primary germline cell distinguishes itself from adjoining nucellar cells, *MADS31* transcript and protein accumulate in the nucellar cells adjacent to the archesporial cell. As the archesporial cell develops into the megaspore mother cell (MMC; Ov3) and undergoes meiosis (Ov4) and mitosis (Ov7/8) to form the embryo sac, MADS31 expression gradually spreads to two or three cell layers of the nucellus that surround the germline, in a zone hereafter referred to as the inner nucellus. In ovules approaching maturity (Ov9b/10), MADS31 was also observed in the outer nucellus, which surrounds the inner nucellus (Fig. 1c). Consistent with the laser capture microdissection (LCM) data, MADS31 expression was also weakly detected in part of the inner integument adjacent to the nucellus apex/micropyle and ovary wall (Fig. 1c and Extended Data Fig. 1c). *MADS31* transcripts were also detected in the embryo sac by LCM–RNA-sequencing as well as in situ hybridization, but no GFP signal could be observed within the germline at any stage. This suggests that MADS31 protein is restricted to somatic cells, and its expression distinguishes the inner from the outer nucellus until ovule maturity.

The inner nucellus and embryo sac are abnormal in *mads31*

To investigate the role of *MADS31* in nucellus development, we used CRISPR/Cas9 gene editing[41] to generate loss-of-function alleles in barley cultivar Golden Promise. Four alleles were identified, incorporating a range of insertions and deletions that compromise production of full-length MADS31 protein (Extended Data Fig. 3a). All four alleles showed a similar reduction in seed set (Extended Data Fig. 3b),

https://doi.org/10.1038/s41477-025-01915-z

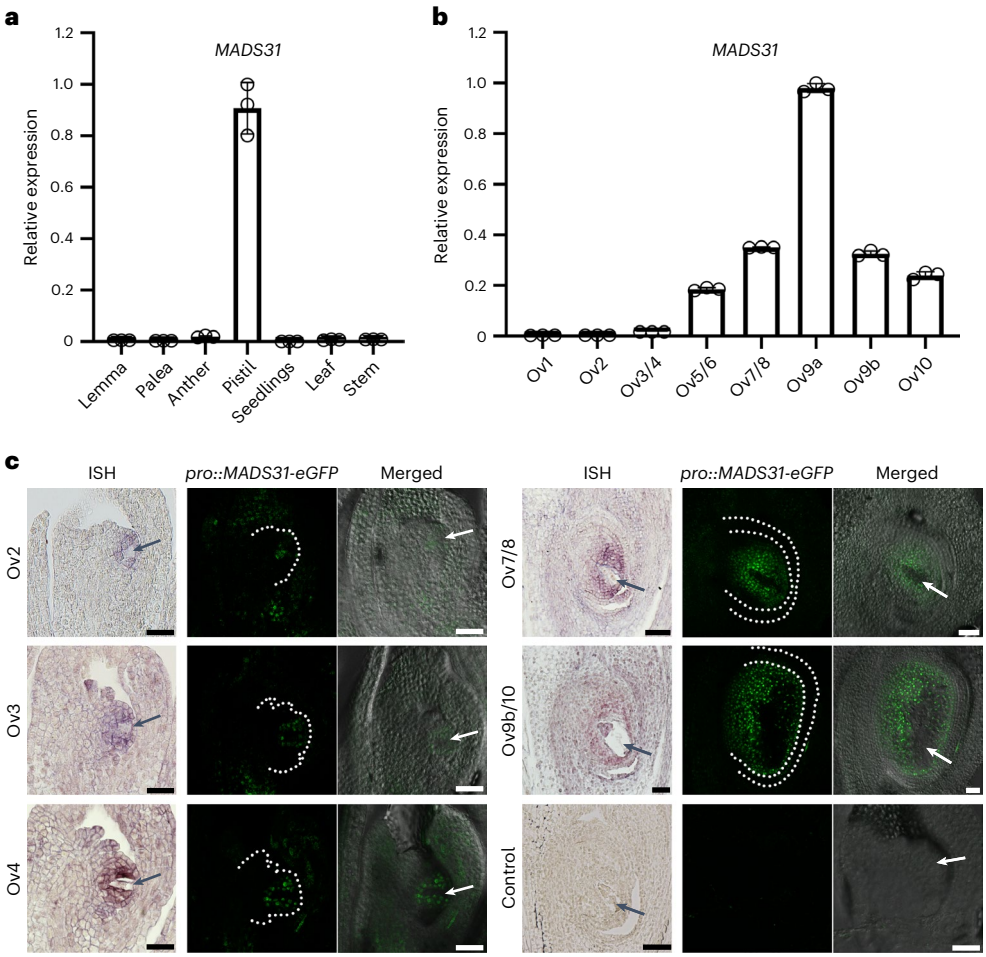

Fig. 1 | *MADS31* is expressed in a restricted niche in the nucellus of barley ovules. **a**, Relative expression level (RT–qPCR) of *MADS31* in vegetative tissues and floral organs. Data are shown as mean ± s.d.; $n = 3$ replicates. **b**, Relative expression level of *MADS31* during ovule development. Ov1, ovule primordium stage; Ov2, archesporial cell stage; Ov3/4, megaspore mother cell/meiosis stage; Ov5/6, functional megaspore stage; Ov7/8, female gametophyte mitosis stage; Ov9a, mature female gametophyte (FG) stage; Ov9b, embryo sac expansion stage; Ov10, anthesis stage. For Ov1–Ov3/4 stages, spikes were collected for RNA extraction. For Ov7/8–Ov10 stages, pistils were dissected from spikelets for RNA extraction. Data are shown as mean ± s.d.; $n = 3$ replicates. **c**, Accumulation of *MADS31* transcripts and MADS31-eGFP fusion proteins shown by in situ hybridization (ISH) and vibratome sections of *pro::MADS31-eGFP* plants, respectively. Black and white arrows indicate the megaspore mother cell (MMC) or FG. White dotted lines indicate the outlines of nucellus and integuments. Ov2, archesporial cell stage; Ov3, MMC stage; Ov4, meiosis stage. Ov9b, FG expansion stage. Sense probe (Ov7/8) and non-transgenic plants (Ov3) served as negative controls. Scale bars, 50 µm. All experiments were repeated 3 times, with similar results.

and one of these was selected (insertion of T) for detailed investigation, hereafter referred to as *mads31*. Compared with wild type (WT), *mads31* spikes produced approximately 50–60% less seeds, verified over two successive generations (Extended Data Fig. 3c). Clearing of mature pistils showed that *mads31* ovules produce smaller embryo sacs, approximately half the size of that in wild type (Extended Data Fig. 3d,e). At anthesis, *mads31* pistils appeared normal in terms of ovary size, style morphology and stigma formation. Furthermore, mature anthers from *mads31* spikelets were yellow and produced viable pollen, indistinguishable from wild type (Extended Data Fig. 3f). These results suggest that reduced seed set in *mads31* is probably a consequence of defective ovule development.

We further examined wild-type and *mads31* ovules using histological sectioning. In wild-type ovules at Ov2 stage, one cell beneath the nucellus apex was enlarged and trapezoid in shape, indicative of the germline archesporial cell (Fig. 2a). The hypodermal nucellar cells that normally express *MADS31* (Fig. 1c) adjacent to the germline were rectangular and aligned uniformly (Fig. 2a). Immunolabelling showed that these cells are labelled by the LM19 antibody, which recognizes de-esterified homogalacturonan (pectin) in the cell wall, and is a potential hallmark of cell wall stiffness[39] (Fig. 2a). On the basis of their position close to the germline, we defined these cells as the inner nucellus. At the same stage in *mads31* ovules, the inner nucellar cells were deformed, rounded and disorganized relative to wild type in over half of the observed ovules. In addition, the accumulation of de-esterified pectin was heavily reduced (Fig. 2a).

At stage Ov3, when the germline differentiates into an MMC in wild-type ovules, the rectangular inner nucellar cells retained de-esterified pectin in their walls but had divided to form a multilayered tissue (Fig. 2b). The same region in *mads31* ovules showed varying degrees of abnormality and was defined by cells of irregular shape that contained low levels of de-esterified pectin in their cell walls (Fig. 2b and Extended Data Fig. 4a,b). After megaspore selection and the initiation of embryo sac mitosis, the innermost cells of the nucellus in wild-type ovules exhibited mild vacuolation consistent with cell degeneration. This vacuolation of inner nucellar cells was more obvious in *mads31* ovules and extended further outwards into the nucellar tissue (Fig. 2c,d and Extended Data Fig. 4c,d). A terminal deoxynucleotidyl transferase dUTP nick-end labelling (TUNEL) assay confirmed additional cell death events within the nucellus of *mads31* relative to wild type (Fig. 2d), suggesting that changes in cell shape and vacuolation in *mads31* might correspond to changes in cell identity and/or viability.

https://doi.org/10.1038/s41477-025-01915-z

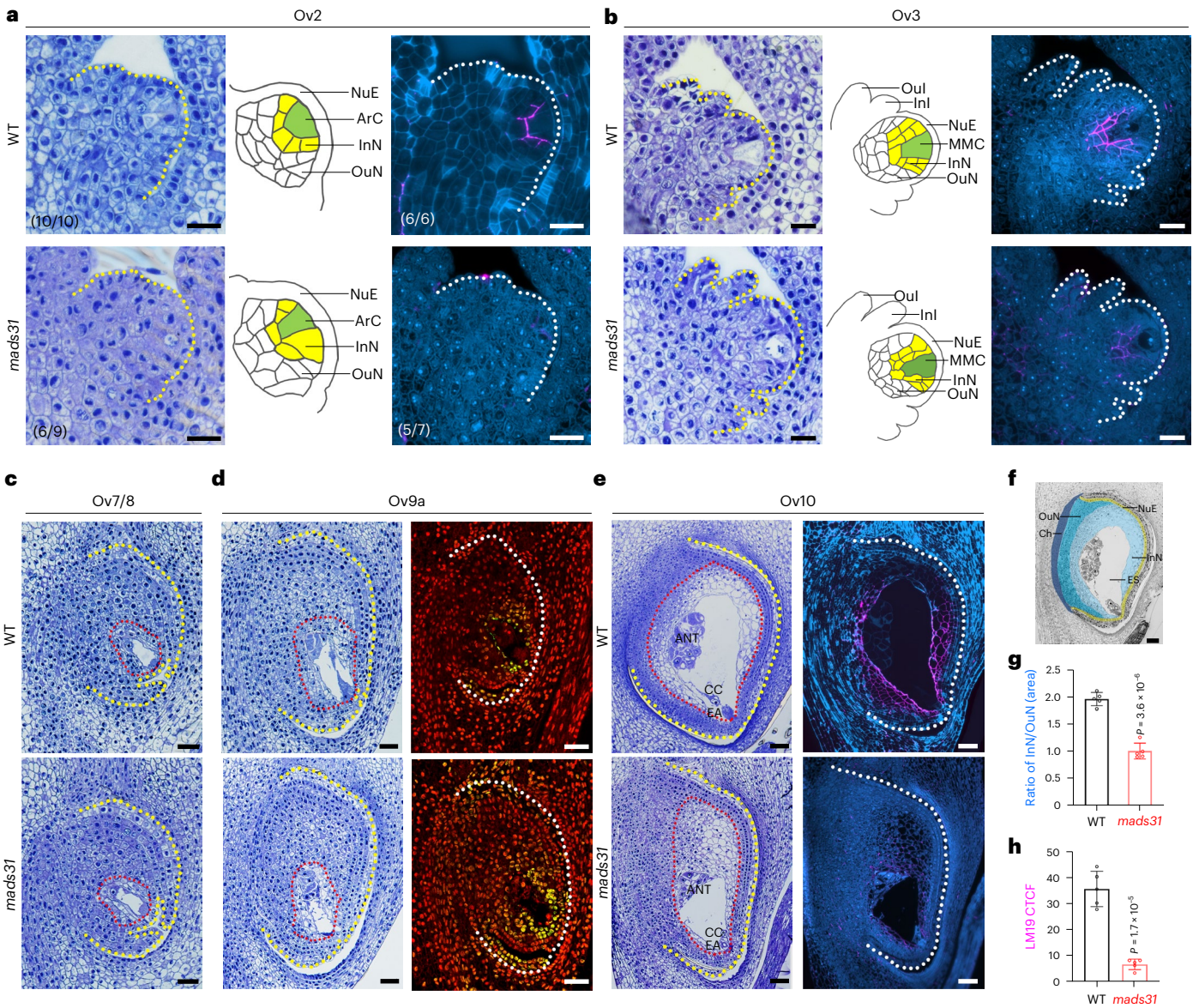

Fig. 2 | Inner nucellus and embryo sac development are impaired in *mads31* ovules. a,**b**, Early stages (Ov2 and Ov3) of ovule development in WT and *mads31*. Left: toluidine blue-stained longitudinal sections of WT and *mads31* ovules. Middle: diagrams of cell arrangement in the nucellus. Green, germ cell; yellow, inner nucellus. Yellow and white dotted lines indicate the ovule within the carpel. Right: LM19-labelled demethylesterified pectin in the cell walls of inner nucellus. OuI, outer integuments; InI, inner integuments; NuE, nucellus epidermis; ArC, archesporial cell; InN, inner nucellus; OuN, outer nucellus. Scale bars, 25 µm. **c**,**d**, Middle stages (Ov7/8 and Ov9a) of ovules in WT and *mads31*. In **d**, Left: toluidine blue-stained longitudinal sections. Right: TUNEL assay in WT and *mads31* ovules. Scale bars, 50 µm. **e**, The final stage (Ov10) of ovules in WT and *mads31*. Left: toluidine blue-stained longitudinal sections. Right: LM19-labelled demethylesterified pectin in the cell walls of inner nucellus. Yellow and white dotted lines indicate the ovule within the carpel and red dotted lines indicate the region of the inner nucellus. ANT, antipodal cells; CC, central cell; EA, egg apparatus. Scale bars, 50 µm. Representative images are shown from sections of >5 ovules; TUNEL and LM19 labelling were repeated 3 times with >5 ovules in each experiment, with similar results. **f**,**g**, Coloured regions of nucellus from semi-thin section (**f**) and statistical analysis for the ratio of inner nucellus area versus outer nucellus (**g**). ES, embryo sac/female gametophyte; Ch, chalaza. Scale bar, 50 µm. Data are shown as mean ± s.d.; $n = 5$ ovules; two-sided t-test. **h**, CTCF of LM19 immunosignals in the nucellus of wild-type and *mads31* ovules. Data are shown as mean ± s.d.; $n = 5$ ovules; two-sided t-test.

In wild-type plants, female germline maturity is attained at stage Ov10 when the ovule contains a fully expanded embryo sac. The mature embryo sac incorporates a cluster of antipodal cells at the chalazal pole, a central cell that is located between the chalazal and micropylar poles, and an egg apparatus that is located at the micropylar pole. At this stage in wild-type ovules, differences between the inner and outer nucellus become more striking. Inner nucellar cells are enlarged, lack obvious cytoplasm, and their walls are rich in de-esterified pectin, whereas those of the outer nucellus are more rounded, contain dense cytoplasm and lack de-esterified pectin (Fig. 2e and Extended Data Fig. 4e). In *mads31*, the embryo sac was typically much smaller (approximately half as large; Extended Data Fig. 3e), containing the residue of degenerated antipodal cells or morphologically abnormal antipodal cells with cytoplasmic condensation as a sign of cellular degeneration (Fig. 2e and Extended Data Fig. 4f). The central cell nucleus was sometimes observed to be directly adjacent to the embryo sac wall or present at the basal micropylar end, and the egg apparatus was mildly vacuolated. In terms of somatic ovule tissues, *mads31* exhibited a larger proportion of outer nucellus relative to inner nucellus (Fig. 2f,g). The small outer nucellus cells appeared to have overproliferated, taking up

https://doi.org/10.1038/s41477-025-01915-z

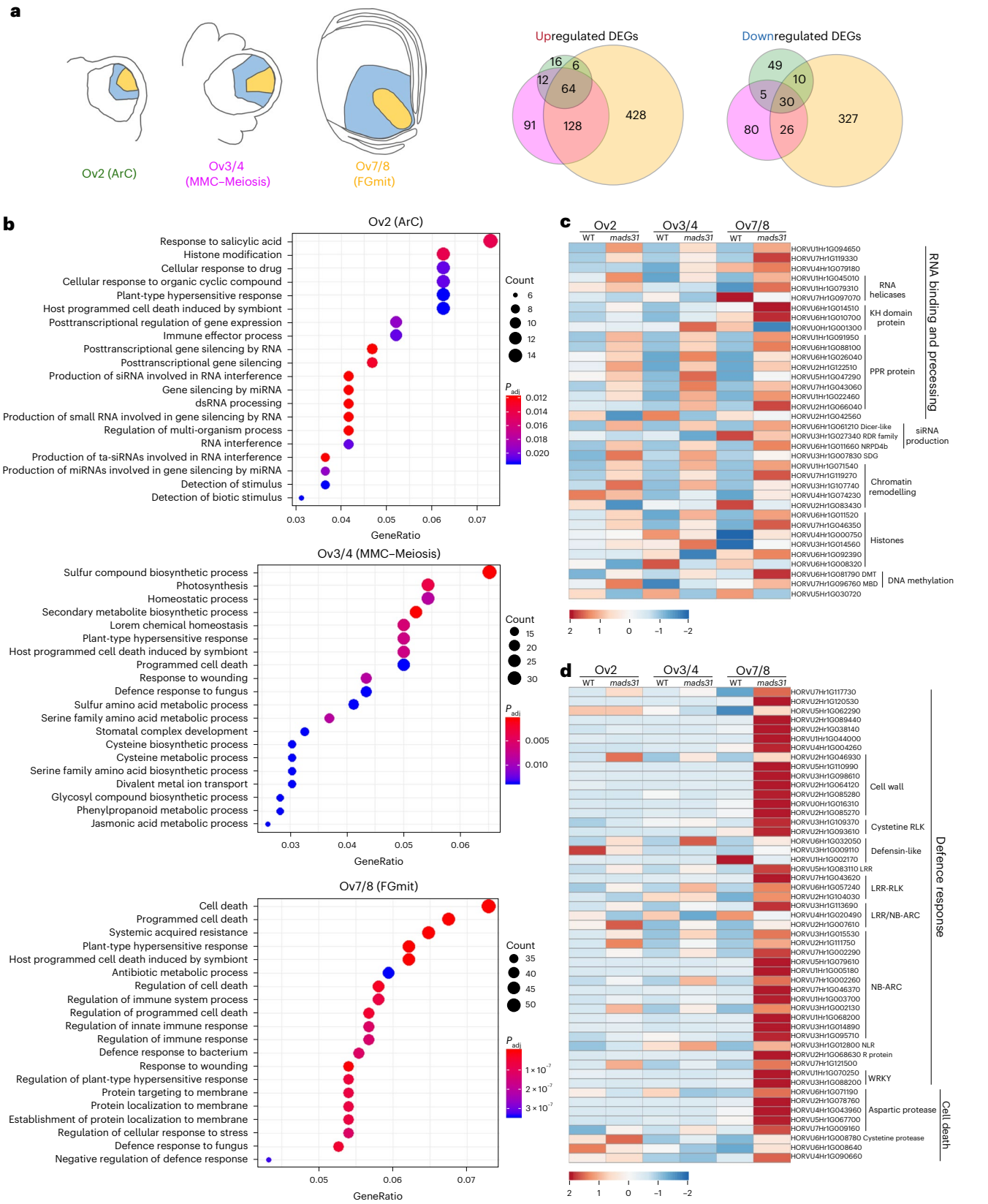

Fig. 3 | Activation of epigenetic pathways and cell death control in *mads31* ovules. a, Ovule stage diagram (left) and Venn diagram (right) representing the overlaps of all upregulated and downregulated DEGs identified from three developmental stages. **b**, GO enrichment of DEGs in Ov2, Ov3/4 and Ov7/8 stages. The Benjamini–Yekutieli method was used for multitest adjustment to correct the *P* values. **c**,**d**, Heat maps of DEGs relevant to post-transcriptional and epigenetic regulation (**c**) and cell death control (**d**). Colour bars show the normalized expression value. KH domain, K homology domain; PPR, pentatricopeptide repeat; siRNA, small interfering RNA; RDR, RNA-dependent RNA polymerase; SDG, SET domain group protein; DMT, DNA methyltransferase; MBD, methylcytosine binding domain; RLK, receptor-like kinase; LRR, leucine-rich repeat; NB-ARC, nucleotide-binding adaptor; NLR, nucleotide-binding domain leucine-rich repeat containing.

much of the room in the ovule. Also, LM19 immunolabelling revealed a significant reduction in the amount of de-esterified pectin, which normally marks cell walls of the inner nucellar cells (Fig. 2e,h). This feature was consistently observed in multiple alleles including *mads31-2, mads31-3* and *mads31-4;* all displayed a deformed inner nucellus and reduced abundance of de-esterified pectin (Extended Data Fig. 5). Importantly, ~25% of *mads31* ovules exhibited less severe morphological changes and appeared WT-like (Extended Data Fig. 4b,f). Given that *mads31* can still produce a reduced number of viable seeds, it is likely that these ovules are the only ones that can be fertilized.

Taken together, these results demonstrate that nucellus differentiation and patterning in barley can be observed at germline initiation and continues until ovule maturity. Loss of MADS31 function impairs the development of the inner nucellus by altering cell morphogenesis and causing premature cellular degeneration. Although MADS31 protein is absent from the germline cells, the embryo sac of *mads31* ovules exhibits defects, consistent with the inner nucellus having an influence on germline development.

Specific pathways are deregulated in *mads31*

To further understand the molecular basis for MADS31 function, we compared the transcriptomes of wild type and *mads31* at several stages by RNA-sequencing. Immature spikes including ovules at stage Ov2 and Ov3/4 were selected to investigate transcriptional changes during megasporogenesis, whereas pistils at stage Ov7/8 stage were selected to investigate changes during gametogenesis. In total, 1,263 differentially expressed genes (DEGs) were identified. At Ov2 stage, only 192 DEGs were found, including 98 upregulated and 94 downregulated DEGs. At stages Ov3/4 and Ov7/8, the number of DEGs increased and the majority were upregulated (67.7% of 436 DEGs and 61.4% of 1,019 DEGs, respectively; Fig. 3a, Extended Data Fig. 6a and Supplementary Dataset 2), suggesting that loss of MADS31 may trigger transcriptional activation. Gene ontology (GO) enrichment analysis indicated that DEGs involved in gene silencing, RNA processing, stress response and cell death control were altered throughout all stages. At stages Ov3/4 and Ov7/8, over 60 DEGs related to metabolic processes, transmembrane transport and cell wall remodelling were also enriched (Fig. 3b and Supplementary Dataset 5).

The prominence of gene silencing pathway genes in the DEG lists was of particular interest, since their deregulation has been reported to induce changes in cell proliferation, cell identity and tissue development in many species[42]. DEGs encoding proteins that can bind and process RNA, such as RNA helicases, K homology domain proteins and pentatricopeptide repeat proteins, were predominantly upregulated in *mads31*, consistent with hyperactive post-transcriptional regulation. Moreover, genes encoding members of the small interfering RNA (siRNA) biosynthetic machinery, such as Dicer-like proteins and NPRD4b, along with factors involved in DNA methylation, histone methylation and chromatin remodelling were also upregulated (Fig. 3c and Supplementary Dataset 3).

In terms of stress response and cell death-related pathways, upregulated genes included executors of cell death, such as aspartic proteases and cysteine proteases (Fig. 3d and Supplementary Dataset 4). Upregulation of these genes at stage Ov7/8 coincided with increased vacuolation of the inner nucellus of *mads31* ovules, which is often a hallmark of cell death[43]. Other genes that were upregulated included two *WRKY* genes, which participate in biotic and abiotic stress responses[44], and genes encoding proteins involved in plant immunity, such as defensins, receptor-like kinases, NB-ARC domain proteins and cell wall remodelling proteins[45]. Transcription factors from multiple families were also upregulated (Extended Data Fig. 5b), including a B3 protein and a basic helix-loop-helix (bHLH) protein, which may indicate a cascade of transcriptional deregulation downstream of MADS31. We verified a number of these DEGs by RT–qPCR in spikes/pistils from wild type and *mads31*. For example, consistent with the cell death detected by TUNEL assay in later stages, we showed that three genes encoding an aspartic protease, NB-ARC protein and a WRKY transcription factor were upregulated during later stages of ovule development (Ov9a and Ov9b), suggestive of prolonged defence and programmed cell death activity in *mads31* (Extended Data Fig. 6b).

In summary, loss of MADS31 appears to trigger transcriptional activation of several pathways, particularly those involved in post-transcriptional regulation, epigenetic regulation, metabolism, defence response and cell death.

MADS31 acts to repress the post-fertilization programme

To confirm whether MADS31 can function as a repressive transcription factor in planta, we cloned promoters from five upregulated DEGs and one downregulated DEG (HORVU3Hr1G061400) that are predicted to carry MADS TF-binding CArG motifs[46]. The activity of the promoter fragments was analysed in the presence of MADS31 via a dual-luciferase assay, along with a control promoter without any CArG motif (proHORVU2Hr1G123460). Expression of MADS31 led to transcriptional repression of all six promoters containing CArG motifs, irrespective of whether the DEG was upregulated or downregulated in the *mads31* RNA-sequencing dataset. Moreover, the number and position of the CArG motifs had minimal impact on the degree of MADS31-induced repression (Fig. 4a). Hence, in this heterologous system, MADS31 appears to be a transcriptional repressor that can act on promoters containing CArG motifs.

Next, we examined the temporal expression profile of DEGs that are usually repressed by MADS31. Remarkably, of the 626 DEGs upregulated in *mads31* pistils at Ov7/8, 51% (354) appeared to be grain-related genes predominantly expressed after fertilization in wild-type plants[38,47] (Supplementary Dataset 5). GO enrichment analysis of these 354 DEGs suggested that multiple grain pathways are precociously activated during pre-fertilization pistil development in *mads31*, including genes involved in protein modification, transmembrane transport and phosphorus metabolism (Supplementary Dataset 6). A representative subset (94) of these genes with preferential expression in the grain is shown in Fig. 4b, which highlights their distinct upregulation after fertilization in wild type. By mapping this subset of 94 upregulated DEGs to the grain LCM transcript dataset, we identified multiple aleurone- and endosperm-enriched genes, including *NRPD4b* (HORVU6Hr1G011660) and *Defensin* (HORVU6Hr1G032050) (highlighted in Fig. 4c). In addition, five sugar transporters and six sulfotransferases that are typically expressed in the post-fertilization pericarp are activated in unfertilized *mads31* pistils (Supplementary Dataset 5). Based on the documented stages of grain development in barley[48], these DEGs are expressed in *mads31* pistils at least 30 days before they would normally be activated during grain development in wild-type plants. This is consistent with MADS31 repressing transcription of a subclass of genes involved in post-fertilization development, many of which are involved in active cell metabolism.

Increased MADS31 modifies nucellar cell identity

The *mads31* loss of function data led us to consider the effect of increased MADS31 expression. To achieve this, the *MADS31* coding sequence was fused to the well-described constitutive *Ubiquitin 1* promoter of maize, which is expressed throughout the plant including in pistils and grain. Regeneration of transgenic *Ubi::MADS31* plants from calli was severely inhibited compared with other constructs, despite multiple attempts. Only two *Ubi::MADS31* lines were regenerated, and these showed severe growth retardation. Even after 40 days of growth in soil, *Ubi::MADS31* plants exhibited excessively curled thin leaves, an absence of tillering and extreme dwarfism typified by a height of only ~2 cm. After 120 days of growth, transgenic plants failed to produce any inflorescence and ultimately withered and died (Extended Data Fig. 7a). This suggests that MADS31 may act as a general repressor of growth, even beyond the ovule.

We also generated *pro::MADS31-eGFP* transgenic plants in the *mads31* and wild-type background. Importantly, *pro::MADS31-eGFP* was confirmed to be functional via complementation of the *mads31* mutant.

https://doi.org/10.1038/s41477-025-01915-z

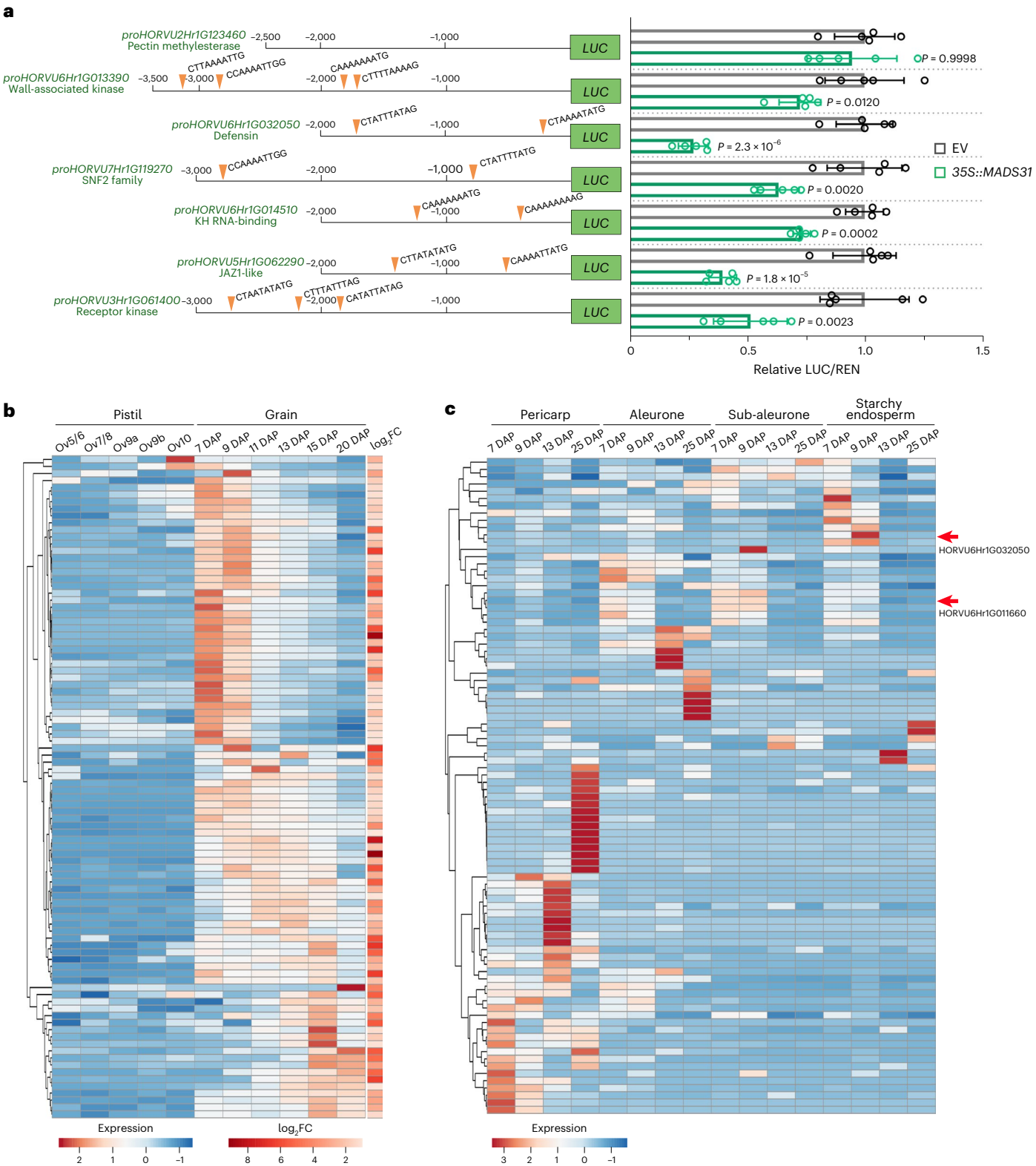

Fig. 4 | *MADS31* represses the post-fertilization programme and maintains embryo sac development. a, Normalized luciferase activity (LUC/REN) regulated by promoters containing CArG motifs in the presence of MADS31 or empty vector (EV, negative control). Data are shown as mean ± s.d.; $n = 5$ replicates; two-sided *t*-test. **b**, Heat map representation of the expression patterns of 94 upregulated DEGs in wild-type pistils and grain. Ov5/6, functional megaspore stage; DAP, days after pollination; FC, fold change. The 'log$_2$FC' column indicates relative gene expression changes (that is, upregulation) in *mads31*, in comparison to wild type. **c**, Heat map representation of the expression patterns of DEGs of **b** in wild-type grain. Gene lists related to **b** and **c** are included in Supplementary Dataset 5.

Three *pro::MADS31-eGFP mads31*/- lines expressing MADS31-eGFP (Extended Data Fig. 7g) exhibited a wild-type phenotype in which no fertility defects or abnormal nucellus patterning were observed (Extended Data Fig. 7h–j). By contrast, extra copies of *MADS31* in a wild-type background, induced prominent changes in ovule development. An examination of mature (Ov10) ovules revealed that compared with

https://doi.org/10.1038/s41477-025-01915-z

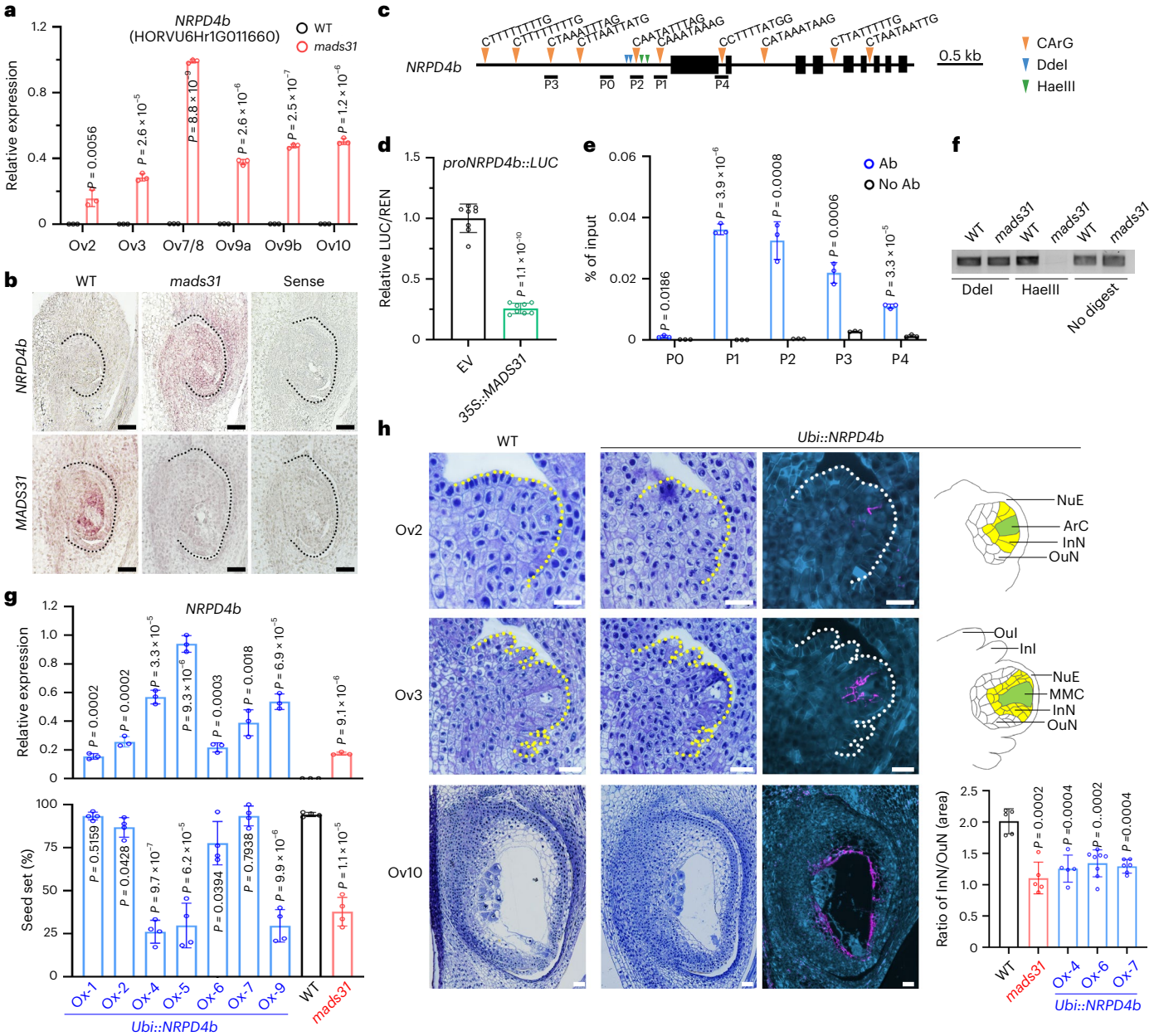

Fig. 5 | MADS31 maintains inner nucellus identity by repressing *NRPD4b* expression in the ovule. a, Relative expression level (RT–qPCR) of *NRPD4b* in WT and *mads31*. Data are shown as mean ± s.d.; $n = 3$ replicates; two-sided *t*-test. **b**, In situ hybridization of *NRPD4b* in WT and *mads31* ovules. The black dotted lines indicate ovules. Sense probe serves as negative control. Scale bars, 50 µm. **c**, The genomic region of *NRPD4b* including promoter and coding region. CArG motifs and restriction enzyme sites are marked. **d**, Normalized luciferase activity (LUC/REN) regulated by *NRPD4b* promoter in the presence of MADS31 or empty vector (EV, negative control). Data are shown as mean ± s.d.; $n = 8$ replicates; two-sided *t*-test. **e**, Four DNA fragments with CArG motif and one without CArG motif tested by ChIP–PCR. No antibody (ab) serves as negative control. Data are shown as mean ± s.d.; $n = 3$ replicates; two-sided *t*-test. **f**, Chop–PCR assay of DNA methylation in *NRPD4b* promoter in WT and *mads31*. Experiments were repeated 3 times, with similar results. **g**, Overexpression of *NRPD4b* decreases seed set rate. Top: relative expression level of *NRPD4b* in transgenic lines, wild-type and *mads31* pistils at Ov7/8 stages. Data are shown as mean ± s.d.; $n = 3$ replicates. Bottom: seeds set rates of transgenic, wild-type and *mads31* plants. Data are shown as mean ± s.d.; $n = 4$ spikes; two-sided *t*-test for unpaired two-sample data. **h**, Early (Ov2 and Ov3) and mature (Ov10) stages of wild-type and *Ubi::NRPD4b* ovules. For *Ubi::NRPD4b*, Left: toluidine blue-stained longitudinal sections. Middle: LM19-labelled demethylesterified pectin in the cell walls of inner nucellus. Right: diagrams of cell arrangement in the nucellus. Green, germ cell; yellow, inner nucellus. Ratios of area of inner nucellus versus outer nucellus are shown as mean ± s.d.; $n = 5$ ovules; two-sided *t*-test for unpaired two-sample data. Scale bars, 25 µm. All experiments were repeated at least 3 times, with similar results.

wild-type ovules at the same stage, *pro::MADS31-eGFP* WT ovules exhibited a greater proportion of nucellar cells with characteristics typical of the inner nucellus, such as larger cell size, compressed cytoplasm and de-esterified homogalacturonan labelling in cell walls, leading to an increased ratio of inner nucellus versus outer nucellus (Extended Data Fig. 7b–d). This suggests that increased MADS31 expression can promote inner nucellus identity in the ovule.

In addition, multiple *pro::MADS31-eGFP* lines in a wild-type background exhibited various degrees of dwarfism coupled with flag leaf inclination (Extended Data Fig. 7e,f), showing architectural similarities to *dicer-like 3* (ref. 49) and *osnrpd1ab*[50] mutants in rice, and suggesting a possible interaction with gene silencing pathways. This is in agreement with the ovule defects, where *mads31* phenotypes are reminiscent of RdDM-related *argonaute* mutants from maize and *Arabidopsis*

that show altered cell identity[10,51]. Taken together, the *mads31* and *pro::MADS31-eGFP* data support the hypothesis that the amount of MADS31 expression affects ovule development through the regulation of inner nucellus identity, and changes in MADS31 expression may interfere with epigenetic regulatory pathways.

MADS31 represses the seed gene *NRPD4b*

Over 30 genes involved in post-transcriptional and epigenetic pathways were identified as DEGs in the *mads31* RNA-seq data (Fig. 3c), including factors involved in siRNA biogenesis, DNA methylation and chromatin regulation. One of these, *NRPD4b*, encodes the fourth largest subunit of RNA polymerase complex IV and V. In *Arabidopsis*, *NRPD4* functions as part of Pol IV/V to enforce transcriptional gene silencing via RdDM[52]. The barley genome contains two copies of the *NRPD4* gene, *NRPD4a* (HORVU6Hr1G071930) and *NRPD4b* (HORVU6Hr1G011660). *NRPD4a* is widely expressed in pistils and grains, while *NRPD4b* is only expressed in grains (Extended Data Fig. 8a). At the tissue level, LCM-transcript profiling revealed that *NRPD4a* transcripts accumulate in all tissues dissected from ovules and grains, but *NRPD4b* is exclusively expressed post fertilization, mainly in the starchy endosperm and aleurone (Extended Data Fig. 8b; refs. 38,47).

Quantitative PCR confirmed that *NRPD4b* transcripts were almost undetectable in wild-type barley pistils, but accumulated to high levels in *mads31* pistils of all stages (Fig. 5a and Extended Data Fig. 8c). Similarly, in situ hybridization of *NRPD4b* detected no expression in the wild-type ovule, while the *mads31* ovule exhibited high *NRPD4b* expression in the nucellus, especially at the micropylar end, with weaker expression in the ovary wall. This overlaps with the expression pattern of *MADS31* in WT ovules (Fig. 5b). Detailed analysis of the *NRPD4b* locus revealed that the putative promoter sequence and introns harbour 10 CArG motifs (Fig. 5c) that are recognized by MADS-box transcription factors. Using a heterologous system, MADS31 protein was able to significantly repress transcriptional activity of the *NRPD4b* promoter in a dual-luciferase assay (Fig. 5d). This was also confirmed by chromatin immunoprecipitation (ChIP)–PCR in *pro::MADS31-eGFP* transgenic plants, which showed that MADS31 directly binds CArG motifs adjacent to the *NRPD4b* start codon (Fig. 5e). Specific DNA regions flanking the CArG motifs also appeared to be affected by the lack of MADS31. A Chop–PCR (DNA methylation-sensitive restriction endonuclease digestion followed by PCR) assay identified a loss of DNA methylation in methylation-sensitive *HaeIII* sites close to one of the *NRPD4b* CArG motifs bound by MADS31, which may contribute to the steady derepression of *NRPD4b* throughout ovary development (Fig. 5f). These results suggest that MADS31 probably acts to directly repress *NRPD4b* transcription in the ovule.

To test whether deregulated *NRPD4b* might contribute to the phenotypes observed in *mads31* mutants, we attempted to uncouple regulation of the *NRPD4b* gene from MADS31. To achieve this, we created transgenic *Ubi::NRPD4b* plants that overexpress the *NRPD4b* coding sequence driven by the *Ubiquitin 1* promoter in a wild-type background. The resulting lines exhibited lower seed set compared with wild type, similar to that observed in *mads31* (Fig. 5g). Moreover, in lines showing abundant *NRPD4b* overexpression, ovules exhibited *mads31*-like phenotypes, as typified by inner nucellar cells being irregular in shape, disorganized and containing reduced de-esterified pectin in their cell walls at stages Ov2 and Ov3 (Fig. 5h and Extended Data Fig. 8d). At maturity (Ov10), *Ubi::NRPD4* transgenic ovules showed altered patterning with an increased ratio of outer nucellus versus inner nucellus cells, and less nucellar cells labelled by LM19, albeit more than that in *mads31* (Fig. 5h and Extended Data Fig. 8e). Thus, *Ubi::NRPD4b* plants show phenotypes in the ovule that are remarkably similar to those observed in *mads31* (Fig. 5h).

Loss of *NRPD4* function in *Arabidopsis* leads to reduced 24-nt siRNA levels and reduced DNA methylation at RdDM target loci, although developmental phenotypes were not reported[52]. We therefore profiled small RNAs (sRNAs) in the Ov7/8 pistils of wild-type, *mads31* and *Ubi::NRPD4b* using sRNA sequencing. While sRNAs shorter than 24 nt were less abundant and sRNAs longer than 24 nt were more abundant in two out of three replicates of *mads31*, the proportion of 24-nt siRNAs was not significantly altered overall in *mads31* and *Ubi::NRPD4b* compared to wild-type (Extended Data Fig. 9a). Given that *NRPD4b* expression is only modified in a subset of *mads31* ovule tissues, cell sorting of nucellus cells followed by sRNA sequencing and DNA methylation analysis might be required to reveal any significant differences, and this is currently technically challenging to address in barley. In parallel, we mapped 24-nt siRNAs to the barley genome. Putative 24-nt siRNA targets were annotated by location (that is, gene body, gene flanking regions and intergenic regions) and feature (that is, transposable element; Extended Data Fig. 9b and Supplementary Dataset 7). Cross-referencing of these regions with 1,019 *mads31* DEGs (at stage Ov7/8) revealed significant enrichment of 24 nt associated features upstream of the transcriptional start site and downstream of the transcriptional termination site, relative to background (Extended Data Fig. 9c). Thus, future studies aimed at decoding the role of 24-nt siRNAs in the MADS31/NRPD4b pathway might consider these loci in detail.

Next, to explore epigenetic marks in *mads31* and *Ubi::NRPD4b* ovules, we also investigated features of histone methylation. As reported above, analysis of the *mads31* transcriptome revealed multiple DEGs involved in chromatin remodelling, and previous studies have implicated these in the control of embryo sac and seed development[53–55]. Histone modifications are routinely examined by immunolabelling (Fig. 6d) and have previously been shown to exhibit different accumulation patterns in distinct ovule cell types of *Arabidopsis*[56,57]. In barley ovules, cells in the inner nucellus surrounding the embryo sac exhibited significantly more H3K9me2 labelling in both *mads31* and *Ubi::NRPD4b* compared with wild-type (Fig. 6e,f), consistent with the deformed inner nucellus in both backgrounds. Conversely, wild-type ovules exhibited an even distribution of H3K27me1 immunolabelling throughout the nucellus, while inner nucellar cells of *mads31* and *Ubi::NRPD4b* showed significantly reduced H3K27me1 labelling (Fig. 6e,f). The similarities in histone labelling patterns in the nucellus of *mads31* and *Ubi::NRPD4b* ovules are consistent with significant changes in inner nucellus identity and provide further support linking the *MADS31* and *NRPD4b* pathways. Moreover, these results confirm that removal of *MADS31* from barley ovules is associated with a range of region-specific epigenetic defects that probably affect the gene expression network across multiple stages of ovule development.

A conserved function of *TaMADS31* in bread wheat

As members of the Triticeae tribe, barley and wheat show similarities during developmental progression of the pistil[48]. To assess whether *MADS31* is conserved in another cereal species, we carried out phylogenetic analysis and identified three putative homeologues in *Triticum aestivum*; *TaMADS31A* (TraesCS2A02G422400), *TaMADS31B* (TraesCS2B02G440900) and *TaMADS31D* (TraesCS2D02G418800) (Fig. 7a). All three *TaMADS31* genes are expressed in the wheat pistil and showed an increase in abundance towards maturity (Fig. 7b). To investigate the function of *TaMADS31* in wheat, we generated a *Tamads31* mutant in cultivar Fielder carrying CRISPR/Cas9-mediated single-base-pair deletions in all three genes (Extended Data Fig. 10a). These mutations are predicted to give rise to truncated Tamads31 proteins via a premature stop codon. Analysis of homozygous *Tamads31* plants revealed a 20–40% reduction in seed set (Extended Data Fig. 10b,c).

Next, we examined wild-type and *Tamads31* ovules using histological sectioning. In contrast to barley, immunohistological staining with LM19 antibody in wheat only showed a low level of de-esterified pectin in the cell walls of the inner nucellus (Extended Data Fig. 10d), possibly because of epitope masking. Conversely, wheat inner nucellus cells could be easily distinguished by calcofluor white (CW) staining,

https://doi.org/10.1038/s41477-025-01915-z

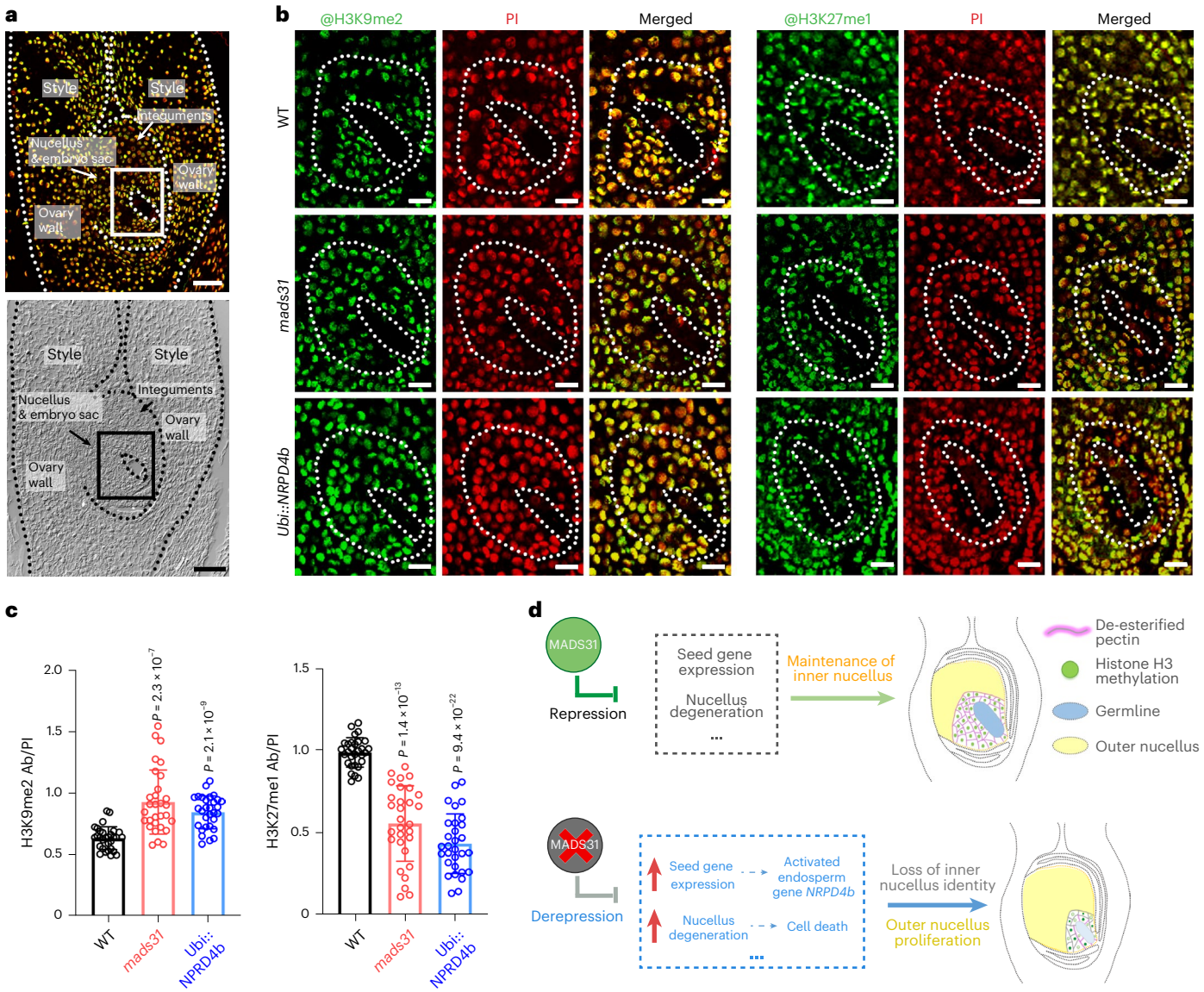

Fig. 6 | Upregulation of *NRPD4b* alters the distribution of histone marks. a, The whole pistil labelled by antibody to detect histone modification in the fluorescent channel (top) and DIC channel (bottom). The white and black rectangles indicate the region of interest shown in **b**. Scale bars, 50 µm. **b**, Immunolabelling of H3K9me2 (left) and H3K27me1 (right) in wild-type, *mads31* and *Ubi::NRPD4b* ovules at Ov7/8 stage. White dotted lines indicate the embryo sac and inner nucellus regions. PI, propidium iodide. Scale bars, 25 µm. **c**, Relative H3K9me2 (left) and H3K27me1 (right) modification levels (measured as antibody signal intensity/DNA signal intensity) in the inner nucellus region of wild-type, *mads31* and *Ubi::NRPD4b* ovules. Data are shown as mean ± s.d.; $n = 30$ nuclei; two-sided *t*-test for unpaired two-sample data. The immunolabelling was repeated 3 times, with similar results. **d**, Proposed model of MADS31 in nucellus patterning. In wild type, MADS31 is preferentially expressed in the inner nucellus, repressing post-fertilization programmes such as seed gene expression and nucellus degradation to maintain the tissue integrity and support embryo sac development. In *mads31* ovules, the lack of repression from MADS31 causes activation of *NRPD4b* and premature cell death, which further alters cell properties and accelerates tissue degeneration, respectively.

possibly due to deposition of (1,3;1,4)-β-glucan or cellulose[58]. From early stage Ov3 to late stage Ov10 in wild type, CW florescence marked the developmental trajectory of the inner nucellus in wild-type wheat ovules (Extended Data Fig. 10c), similar to that of LM19 in barley (Fig. 2). Compared with wild type, *Tamads31* ovules showed altered development of the inner nucellus, evidenced by less cell layers with fluorescent signal and a larger proportion of outer nucellus relative to inner nucellus (Extended Data Fig. 10c–e). With regards to the embryo sac, the antipodal cell cluster was smaller or even absent in *Tamads31* ovules, and mislocated central cell nuclei were also observed, remarkably similar to that observed in barley *mads31* ovules (Extended Data Fig. 10e).

In summary, loss of TaMADS31 function leads to a reduced proportion of inner nucellus relative to outer nucellus, changes in cell wall composition and defects in germline development. This suggests that MADS31 function in supporting inner nucellus development and female fertility is conserved between two different cereal species.

Discussion

In plants, the female germline is enveloped in multiple layers of sporophytic (somatic) tissue, providing diverse sources of regulatory cues for germline development. Cues include cell-autonomous factors acting only in the germline[59], and non-cell-autonomous pathways acting from the nucellus, integuments, funiculus and vascular system[6,60,61]. In terms of local control, the nucellus represents the closest source of somatic information to coordinate germline progression. Although present in all angiosperm ovules, nucellus size, morphology and development

https://doi.org/10.1038/s41477-025-01915-z

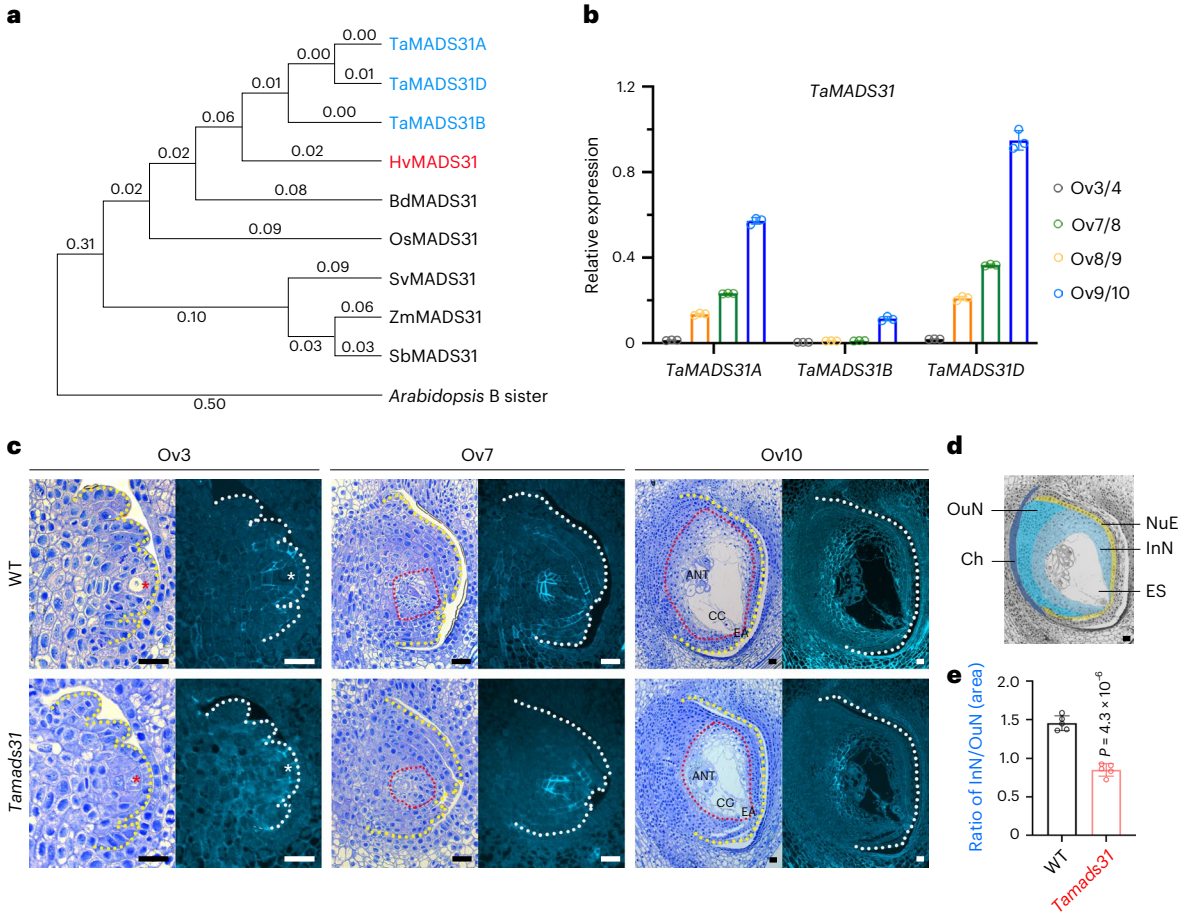

Fig. 7 | TaMADS31 maintains the inner nucellus during ovule development in bread wheat. a, Phylogenetic analysis of MADS31 homologues in small-grained cereals and *Arabidopsis*. Ta, *Triticum aestivum*; Hv, *Hordeum vulgare*; Bd, *Brachypodium distachyon*; Os, *Oryza sativa*; Sv, *Setaria viridis*; Zm, *Zea mays*; Sb, *Sorghum bicolor*. **b**, Relative expression level (RT–qPCR) of *TaMADS31A*, *TaMADS31B* and *TaMADS31D* during ovule development. Data are shown as mean ± s.d.; $n = 3$ replicates. **c**, Early (Ov3), middle (Ov7) and mature (Ov10) stages of ovules in WT and *Tamads31*. Left: toluidine blue-stained longitudinal sections. Right: calcofluor white-stained longitudinal sections. Yellow and white dotted lines indicate the ovule within the carpel and red dotted lines indicate the region of the inner nucellus. Red and white asterisks indicate the megaspore mother cells. Representative images are shown from sections from 3 experiments with >4 ovules in each experiment, with similar results. **d**,**e**, Coloured regions of nucellus from semi-thin section (**d**) and statistical analysis for the ratio of inner nucellus area versus outer nucellus (**e**). Data are shown as mean ± s.d.; $n = 5$ ovules; two-sided *t*-test. Scale bars, 25 µm.

vary considerably between species[1,2,5]. In *Arabidopsis*, for example, the nucellus is prominent during early ovule growth, but degrades quickly and occupies only a small proportion of the ovule after meiosis, leaving room for the integuments to directly enclose the embryo sac[62]. By contrast, cereal ovules exhibit a larger multiple-layered nucellus that surrounds the germline until fertilization, meaning that the integuments have no direct connection to the embryo sac[63]. Previously, we showed that the nucellus of barley can be further differentiated into two zones, the inner nucellus and the outer nucellus, on the basis of their position relative to the germline, their cellular morphology and cell wall organization[39]. MADS31 is a Bsis MADS-box protein that is preferentially expressed in the inner nucellus. The loss of MADS31 leads to changes in gene expression associated with epigenetic regulation and seed development. This coincides with premature cell death and impaired integrity of inner nucellus cells, proliferation of outer nucellus cells and the inhibition of germline development (Fig. 6g). Thus, MADS31 represents a key factor to dissect the role of different nucellus tissues and associated molecular pathways during cereal ovule and seed development.

A recent examination of rice pistil development using single-nucleus RNA sequencing also uncovered a cell cluster located in the 'innermost part of the nucellus'[64]. Indeed, a differentiated 'inner zone' within the nucellus is not unique to Triticeae cereals and has been reported in other angiosperms such as soybean[65] and ginkgo[66], sometimes referred to as a nucellar epithelium[1]. Even in the small nucellus of *Arabidopsis*, transient nucellar cells immediately adjoining the germline appear different from persistent nucellus cells at the chalazal end of the embryo sac, both in terms of morphology and function[67]. How nucellus subdomains maintain their boundaries and relative proportion are largely unknown, and the biological significance of the bond between the subdomains is similarly unclear. It is also unclear how temporal regulation of cell death or cell elimination might contribute to subdomain function and embryo sac expansion. In the *Arabidopsis b-sister* (*abs/tt16*) mutant, proximal nucellar cells appear to persist or even proliferate after fertilization, leading to abnormal chalazal endosperm growth[29]. This role of ABS in promoting cell elimination appears distinct from that of MADS31 which restricts cell death during pre-fertilization stages; however, in both cases the mutant phenotype has an increased ratio of outer to inner nucellus. Hence, although the spatiotemporal aspects of Bsis function may differ, *ABS* and *MADS31* appear to share a similar role in regulating nucellar proportions. Whether an overproliferated outer nucellus affects post-fertilization development in Triticeae cereals similar to that in *Arabidopsis* requires further investigation.

The association between the inner nucellus and female germline also shares noteworthy similarities with that of the tapetum and male

germline in anthers. Both the inner nucellus and tapetum provide a transient interface between somatic and germline tissues, and both undergo precisely controlled cell death, which is required for downstream development[68–70]. Although *MADS31* transcripts are detectable in the embryo sac by LCM–RNA-sequencing and mRNA in situ hybridization, MADS31 protein accumulates in the nucellus but not in the germline (Fig. 1c), suggestive of post-transcriptional regulation of *MADS31* expression. Importantly, defective germline formation in *mads31* mutants correlates with altered inner nucellus development, and expression of MADS31-eGFP fusion protein in the nucellus can rescue the embryo sac development in *mads31* mutants (Extended Data Fig. 7). Hence, MADS31 appears to maintain inner nucellus identity, which is essential for female germline development.

The molecular interplay between the germline and surrounding cells during sporogenesis involves complex epigenetic regulatory activities[6,71]. In *Arabidopsis*, recent findings in the anther suggest that so-called somatic nurse cells in the tapetum provide siRNAs for RdDM activity in the male germline[72]. RdDM pathways are also thought to generate siRNAs in the nucellar cells to coordinate MMC specification[10,51,73,74]. Other epigenetic pathways are also likely to be involved. For example, the Histone H3 methyltransferase *ASH1 HOMOLOG 2* (*ASHH2*) gene is required for both anther and ovule development[75]; the Polycomb proteins RING1A/B coordinate H2A monoubiquitination of genes essential for embryo sac development, such as *AGO5* and *WRKY23* (ref. 76); and two epigenetic factors, the chromatin remodelling complex *SWI2/SNF2-RELATED 1* (*SWR1*) and *SET DOMAIN GROUP 2* (*SDG2*) involved in H3K4me3 histone modification, interact with receptor kinase signalling to regulate female germline progression[77]. In contrast to the array of characterized effectors, remarkably little is known about the upstream transcriptional regulators of epigenetic activities, particularly in an ovule cell-type-specific context. In *Arabidopsis*, the D-class MADS-box gene *STK* was recently shown to activate biogenesis of siRNAs via RDR6 and AGO9 to restrict the expression of *SPOROCYTELESS/NOZZLE*, leading to the specification of a single female germline cell[15]. Here we show that MADS31 is potentially a negative regulator of multiple epigenetic activities in the ovule and acts by directly repressing seed-specific *NRPD4b* expression. Together, this suggests that sophisticated regulation of the epigenetic pathways by different classes of MADS-box genes is an important feature of ovule development.

While Bsis MADS-box genes show relatively low cross-species homology at the protein level, they exist widely in plants that bear female reproductive organs[27,78,79] and are typically expressed in somatic cells of ovules, such as the nucellus, integuments and carpel/ovary wall. In *Arabidopsis*, the two Bsis genes *GOA* and *ABS* are expressed in the nucellus and integuments, but their function in the ovule during pre-fertilization stages appears to be restricted primarily to the integuments[31,32]. In rice and barley, the Bsis gene *MADS29* is also expressed in the nucellus and integuments, but the loss of *MADS29* predominantly results in defects in the nucellus and nucellar projection[22,36]. Here we show that MADS31 regulates inner nucellus development across multiple stages of development in both barley and wheat, also with limited impact on the integuments. We speculate that before fertilization, Bsis genes may have been recruited to regulate the development of tissues directly adjoining the germline, that is, the integuments in tenuinucellar ovules (for example, *Arabidopsis*) and the nucellus in crassinucellar or semi-crassinucellar ovules (for example, barley). Bsis homologues also exhibit an interesting common feature via ectopic expression experiments. Overexpression of *GOA*, *ABS*, Orchid *PeMADS28* and Gingko *GbMADS9* by a constitutive promoter in *Arabidopsis* leads to phenotypes such as dwarfism, abnormal floral organs, early flowering time and sterility[33,34,78,80]. Similarly, transgenic plants overexpressing *OsMADS29* in rice are dwarfed, early flowering and sterile[81]. Here, the overexpression of *MADS31* in barley shows severe negative effects on development, whereby transgenic plants are dramatically stunted and unable to flower. Thus, multiple Bsis class members appear to be negative regulators of growth. Their restricted expression in the ovule may therefore control growth in key zones adjoining the germline and subsequently in nutrient transfer tissues, creating an optimal environment for germline initiation, progression and subsequent nutritional support.

Consistent with its proposed function as a repressor of growth, MADS31 predominantly represses expression of target genes (Fig. 4). The molecular consequences of transcriptional derepression in *mads31* are remarkable and include precocious activation of cell death pathways and seed-specific genes, in unfertilized ovules. This derepression coincides with premature cell death in the inner nucellus, overproliferation of the outer nucellus and rewiring of metabolic pathways. During normal ovule development, fertilization is an important cue for maternal tissue degradation, before the initiation of endosperm and embryo development[63]. The altered nucellus morphology and female sterility in *mads31* may therefore result from the precocious activation of fertilization-triggered programmed cell death. Alternatively, premature expression of seed-specific *NRPD4b* may compromise RNA polymerase complex IV/V function and siRNA pathways, thereby interfering with the function of the inner nucellus as a nurse tissue for the female germline. It is notable that in *mads31* and *Ubi:NRPD4b* lines, ovule defects become progressively worse with time, starting with a loss of inner nucellus identity and evolving to overproliferation of the outer nucellus and abnormal embryo sac development. This array of phenotypes appears consistent with the pleiotropic molecular changes in *mads31*, including transcriptional activation of regulatory genes, derepression of *NRPD4b* and cell-type-specific changes in histone methylation. Although the ovule defects do not appear to be consistently associated with wholesale changes in sRNA abundance, 24-nt siRNA targets are significantly enriched within the flanking regions of *mads31* DEGs identified from transcriptome profiling. These loci may offer further opportunities to explore the regulatory relationship between MADS31 and NRPD4b, but mechanistic insight will probably require improvements in single-cell isolation and profiling to assess their role in specific regions of the nucellus.

MADS-box proteins typically form heteromeric complexes with other MADS-box members to execute function[82] and a physical interaction between OsMADS29 and OsMADS31 suggests that the Bsis class proteins can function in a complex[83]. Although MADS29 targets remain unknown in barley, rice OsMADS29 has been reported to activate nucleotide-binding site–leucine-rich repeat (NBS-LRR) and cysteine proteases involved in stress response and cell degeneration[21,81]. Here we show that similar genes appear to be repressed by MADS31 in barley, raising the possibility that MADS31 and MADS29 act antagonistically in controlling cell death. How this might be achieved in the barley ovule where *MADS31* and *MADS29* are both expressed, remains to be determined. MADS-box proteins have also been shown to interact with chromatin remodelers to regulate their targets[84–86], and the decrease of DNA methylation in the *NRPD4b* promoter region adjoining the CArG motifs reveals a potential link to the epigenetic silencing machinery. Future studies may consider whether MADS31 directly interacts with epigenetic components, as well as regulating them, to reinforce repressive states during reproductive development.

Methods

Plant materials and generation of transgenic plants

The wild-type barley (*Hordeum vulgare* L.) cultivar Golden Promise (GP) was used as a control and donor plant for transgenesis. An optimized CRISPR/Cas9 genome editing system was utilized to generate mutants[41]. Two specific targets were selected for *MADS31* near the start codon. Targets were sequenced in GP to guarantee pairing between single guide RNA (sgRNA) and genomic DNA. SgRNA–target 1 (T1) was driven by rice promoter *OsU6c*, and sgRNA–T2 was driven by rice

promoter *OsU3*. The sgRNA expression cassettes of *OsU6c–sgRNA–T1* and *OsU3–sgRNA–T2* were amplified from pYLsgRNA–OsU6c and pYLsgRNA–OsU3 plasmids using Phusion High-Fidelity DNA Polymerase (New England BioLabs) and cloned into a binary vector, pYLCRISPR–Cas9Pubi-H, using two *BsaI* sites as described.

To trace MADS31 protein accumulation in planta, a ~4 kb genomic DNA fragment including 2.4 kb of promoter and the full genomic coding region of *MADS31* were fused in frame to *eGFP* and inserted between the *HindIII* and *BstEII* sites of pCAMBIA1301, using In-Fusion (Takara) cloning technology. This construct was also used to complement the *mads31* mutant. For *MADS31* overexpression, the full-length *MADS31* coding sequence was inserted into vector pU1301 via *KpnI* and *BamHI* sites behind the maize *Ubiquitin 1* promoter. The same cloning method was used for *NRPD4b* overexpression. All primers used for constructs are listed in Supplementary Table 1.

All constructs were transformed into immature GP or *mads31* embryos using an *Agrobacterium tumefaciens* AGL1-mediated transformation method described previously[87]. All barley plants were grown in cocopeat soil, in 15 °C light,12 °C dark, 16 h daylight with 70% humidity (The Plant Accelerator, Waite Campus, The University of Adelaide, Australia). Individual T_0, T_1 and T_2 plants carrying homozygous or biallelic mutations generated by CRISPR were identified by Sanger sequencing (AGRF) of the targets and flanking region amplified by the Phire Plant Direct PCR kit (ThermoFisher).

The wild-type bread wheat (*Triticum aestivum*) cultivar Fielder was used as a control and donor plant. A modified CRISPR/Cas9 system was used to create *Tamads31* mutants in wheat. Two target sequences (T1 and T2) for sgRNA were selected to edit all three homologues of the *TaMADS31* gene. Target sequences were evaluated by CRISPRdirect (https://crispr.dbcls.jp) in the wheat genome[88]. The target sites were sequenced in Fielder before TaU3-sgRNA-T1 and TaU6-sgRNA-T2 expression cassettes were cloned into a binary vector pBUE411 (ref. 89). The construct was transformed into *A. tumefaciens* strain EHA105. Wheat transformation was performed as previously described[90]. All wheat plants were grown in cocopeat soil, in 24 °C light, 20 °C dark, 16 h daylight with 50% humidity in growth chambers (The Plant Accelerator). Individual plants carrying mutations generated by CRISPR were identified by Sanger sequencing (AGRF) of the targets and flanking region amplified by the Phire Plant Direct PCR kit (ThermoFisher). Primers used for genotyping are listed in Supplementary Table 1.

Plant and pistil phenotyping

Barley plants, spikes, anthers and pistils, and wheat spikes were photographed using a Nikon D5600 digital camera. Mature anthers were dissected from spikelets and crushed on microscopy slides to release pollen grains. Pollen grains were stained in Lugol's iodine for 30 s and photographed using an optical microscope (Ni-E, Nikon). For clearing, whole pistils were collected from spikelets approaching anthesis and fixed in ice-cold formaldehyde-alcohol-acetic acid (FAA) immediately. Pistils were dehydrated in a series of 70, 80, 90 and 100% (v/v) ethanol and cleared in Hoyer's solution for 4 weeks[91]. Cleared pistils were imaged using a Zeiss AxioImager M2 with differential contrast microscopy (DIC).

Fresh spikes (for ovules of Ov2–Ov7/8) or pistils (for ovules of Ov9b/10) were collected from *pro::MADS31-eGFP* plants and embedded in 5% (m/v) agarose blocks immediately. After solidifying and trimming, samples were sectioned into 50–70 µm slices using a Leica Vibratome VT1200. Slices were laid on microscopy slides and mounted using 50% (v/v) glycerol solution. Ovule sections containing the germline were imaged using an A1R laser scanning confocal microscope (Nikon) (eGFP, excitation 488 nm, emission 505–520 nm). Images were processed with NIS-Elements Viewer 4.20 (Nikon). Intact ovules of Ov3–Ov10 were carefully dissected from pistils of *pro::MADS31-eGFP* and *mads31/pro::MADS31-eGFP* plants and photographed with a Zeiss AxioImager M2 (eGFP, excitation 450–490 nm, emission 500–550 nm; auto fluorescence, excitation 335–383 nm, emission 420–470 nm).

Sectioning and pectin immunolabelling

Pistils or whole spikelets from wild-type plants, mutants and transgenic plants were collected and fixed in FAA, dehydrated in a series of 70, 80, 90 and 100% (v/v) ethanol and embedded in Technovit 7100 resin (Kulzer Technique) as described by the manufacturer. Samples were sectioned to a thickness of 1.5 µm on a Leica Ultramicrotome. Sections were stained in 0.5% toluidine blue (w/v) and imaged with a Nikon Ni-E optical microscope. For pectin immunolabelling, unstained sections were incubated with rat antibody LM19 (1:100 dilution, PlantProbes, ELD001), followed by secondary antibody Alexa Fluor 555 conjugated goat anti-rat IgG (1:200 dilution; Invitrogen, A48263)[92]. Then sections were stained in calcofluor white stain (Sigma-Aldrich) for 1 min for background cell wall labelling. After three rinses with water, sections were mounted with 90% glycerol and imaged with a Zeiss AxioImager M2 (LM19, excitation 538–562 nm, emission 570–640 nm; calcofluor stain, excitation 335–383 nm, emission 420–470 nm). Fluorescence intensity was measured using ImageJ. Mean fluorescence of background was measured to calculate corrected total cell fluorescence (CTCF). Tissue areas were measured using ZEN blue edition (Zeiss).

TUNEL assay

Tissues were collected into glass vials and fixed in ice-cold FAA. Plant materials were dehydrated in a series of 70, 80, 90 and 100% (v/v) ethanol and embedded in paraffin. Paraffin sections (8 µm) were prepared using a Leica rotary microtome RM2265 and transferred to polysine coated slides (ThermoFisher), dewaxed, rehydrated and post fixed in 4% (w/v) paraformaldehyde. Nick-end labelling of nuclear DNA fragmentation mediated by terminal deoxynucleotidyl transferase (TdT) was performed following the instructions for the DeadEnd Fluorometric TUNEL System (Promega). Sections were stained in 1 µg ml^{-1} propidium iodide (PI) before mounting in 90% (v/v) glycerol with 25 mg ml^{-1} DABCO (1,4-diazabicyclo[2.2.2]octane), then imaged using an A1R laser scanning confocal microscope (Nikon) (fluorescein-12-dUTP, excitation 395 nm, emission 500–540 nm; PI, excitation 561 nm, emission 590–640 nm) using NIS-Elements AR (Nikon).

RNA extraction and RT–qPCR

Total RNA was extracted from barley and wheat tissues using a Spectrum Plant Total RNA kit (Sigma-Aldrich). Total RNA (2 µg) was purified using the TURBO DNA-free kit to remove genomic DNA. First-strand complementary (c)DNA was generated using SuperScript IV Reverse Transcriptase (Invitrogen) and oligo-dT primer, following manufacturer instructions. Diluted cDNA was used as templates mixed with i*Taq* Universal SYBR Green Supermix (Bio-Rad) for real-time quantitative PCR using a QuantStudio Flex 6 (Life Technologies) machine. *HvACTIN7* and *TaTubulin* were used as housekeeping gene for normalization. All primers used for RT–qPCR are listed in Supplementary Table 1.

RNA in situ hybridization

MADS31 and *NRPD4b*-specific fragments were amplified from cDNA templates by PCR using primers fused with T7 polymerase promoters. PCR products were used as DNA templates for in vitro transcription. Digoxigenin (DIG)-labelled nucleoside triphosphates (NTPs) (Roche) was used to label antisense and sense probes generated by T7 polymerase (ThermoFisher), according to manufacturer instructions. Barley tissues were fixed, embedded and sectioned as described in the TUNEL assay. Rehydration, post fixation, hybridization, stringent washes and immunodetection were automatically performed in an InsituPro VSi robot (Intavis). To visualize hybridization signal, an antibody conjugate anti-DIG-AP (1:1,000 dilution, Roche) and NBT/BCIP substrate were used for colouring reaction. Images were taken with a Nikon Ni-E

optical microscope, using NIS-Elements AR (Nikon). All primers used are listed in Supplementary Table 1.

RNA-sequencing and data analysis

In wild type and *mads31*, for samples of Ov2 and Ov3/4 stages, whole barley spikes at Waddington scale[48] W5.5–6 and W6.5–7 stages, respectively, were collected. Anthers were carefully removed with a dissecting needle. For samples of Ov7/8 stages, pistils at W8.5–8.75 stage were dissected from spikelets. Total RNA was isolated from tissues described above for each of three biological replicates using an RNeasy plant mini kit (Qiagen). RNA quality assessment, libraries preparation and paired-end sequencing were performed at Novogene (Australia). The quality of raw data was examined using FastQC. After trimming adaptors and filtering, clean reads were mapped to the barley reference genome[93] (Morex V1, http://webblast.ipk-gatersleben.de) using HISAT2 aligner. Fragments per kilobase per million (FPKM) were normalized using HTSeq. Genes were considered as differentially expressed at false-discovery rate-adjusted $P < 0.05$ and $\log_2$(fold change) > 1 or < −1. A total of 1,263 DEGs were identified using the R package DESeq2 and further annotated according to BLASTX against protein databases of *Arabidopsis* (https://www.arabidopsis.org) and rice (http://rice.uga.edu). A Venn diagram was created on the basis of DEGs identified. The R package 'clusterProfiler' was utilized for GO enrichment[94]. The Benjamini–Yekutieli method was used for multitest adjustment to correct the *P* values. For gene expression heat maps, the original FPKM or transcripts per million (TPM) values of genes of interest were extracted from RNA-seq data or the LCM–RNA-seq data[38,47]. The expression heat map was created using ClustVis (2.0)[95].

Small RNA-sequencing and data analysis

Pistils at W8.5–8.75 were dissected from spikelets of wild-type, *mads31* and *Ubi::NRPD4b* plants. Total RNA was isolated from each of three replicates using TRIzol reagent (Invitrogen). Small RNA isolation, libraries construction and single-end sequencing were performed at Novogene. For data analysis, raw reads were filtered by removing low-quality reads and adapter containing reads using fastp[96]. Clean reads were mapped to the barley genome (MorexV3_pseudomolecules_assembly) using Bowtie with the unique mapping parameter 'bowtie -q -p 15 -m 1'[97]. Barley transposable elements annotation was collected from the GrainGenes database (https://wheat.pw.usda.gov/GG3/content/morex-v3-files-2021). siRNA targets (24 nt) were filtered out on the basis of mapped fragments length; these 24-nt siRNA targets were then annotated using HOMER (http://homer.ucsd.edu/homer/ngs/customGenomes/index.html). For 24-nt siRNA targets density analysis, we calculated the 24-nt siRNA targets number on the basis of 1 kb genome bins using BEDTools[98], then shuffled the genes on the basis of DEGs with the same number, summarized the 24-nt siRNA targets density from 6 kb upstream to 6 kb downstream of the gene body in DEGs and shuffled gene sets using deeptools[99].

ChIP–PCR

One gram of material including young spikelets (W7.5–8.5) with anthers pinched off, and pistils (W8.75–10) were collected from *pro::MADS31-eGFP* transgenic plants. ChIP was performed following the method previously described by ref. 100. In brief, chromatin was cross-linked, isolated by nuclei lysis and sonicated into ~100–500 bp, centering ~250 bp. Sheared chromatin was pre-cleared using salmon sperm DNA/Protein A/G agarose beads (ThermoFisher) before overnight incubation with anti-GFP antibody (ABclonal, AE012; 1:300 dilution) at 4 °C. The Protein A/G agarose beads were added for a 2 h incubation, then washed in low salt, high salt, LiCl and TE buffer. The beads were washed twice with elution buffer to collect immunocomplexes. Reverse crosslinking was performed in 0.2 M NaCl solution at 65 °C for overnight incubation. DNA was purified using proteinase K digestion, phenol-chloroform-isoamyl alcohol extraction and precipitation with ethanol, sodium acetate (pH 5.2) and glycogen at −80 °C. Purified input and immunoprecipitated DNA were used as templates for qPCR to calculate enrichment. 'No antibody' precipitation was used as negative control. All primers are listed in Supplementary Table 1.

Dual-luciferase assay

Dual-luciferase assay was performed using transient expression in *Nicotiana benthamiana* leaves. An effector plasmid was constructed by inserting the full-length *MADS31* coding region into the *HindIII* and *BamHI* sites of the pGreenII-0000 vector, which drives effector expression by the 35S promoter. A series of promoters of DEGs were amplified from genomic DNA and cloned into the *HindIII* and *BamHI* sites of pGreenII-0800-LUC vector to drive expression of the *LUC* reporter gene. All plasmids including empty vector pGreenII-0000 were co-transformed with helper plasmid pSoup-P19 into *A. tumefaciens* GV3101 cells. Full-strength overnight *Agrobacterium* cultures were collected and resuspended. Each reporter strain was mixed with MADS31 effector strain or empty vector strain at a ratio of 1:4 (v:v). The reporter–effector mixture was infiltrated into young tobacco leaves using a 2 ml syringe, then plants were kept in weak light for 48 h. Leaves were harvested and processed using the Dual-Luciferase Reporter Assay System (Promega), following manufacturer instructions. *Renilla* luciferase was used as an internal control to normalize firefly luciferase. LUC was quenched and the REN reaction initiated by adding 100 µl of Stop and Glow buffer, using a GloMax-96 microplate luminometer (Promega). All primers are listed in Supplementary Table 1.

Chop–PCR

For Chop–PCR, barley genomic DNA was extracted from wild-type and *mads31* pistils (W8–8.75) using the cetyltrimethylammonium bromide method[101]. Genomic DNA (1 µg) was digested overnight with DNA methylation-sensitive restriction endonuclease DdeI and HaeIII (New England BioLabs) and used as a template for PCR reactions utilizing primers flanking the endonuclease recognition sites. DdeI and HaeIII report on CHH and CHG methylation, where H indicates A, T or C. Non-digested genomic DNA served as control. The gel image was taken with a Bio-Rad ChemiDoc imaging system, using Image Lab software (Bio-Rad). All primers are listed in Supplementary Table 1.

Histone immunolabelling

Immunodetection of histone methylation was performed following a previous method with modifications[102]. Tissues were fixed, embedded and sectioned as described in the TUNEL assay. After dewaxing and rehydration, paraffin sections (6 µm) were microwave-heated in 10 mM citrate buffer (pH 6.0) for 5 min at high power for antigen retrieval. Sections were incubated with blocking buffer (3% (m/v) BSA in PBS buffer) for 1 h before overnight incubation with primary antibodies for H3K9me2 (1:400 dilution; abcam, ab1220) and H3K27me1 (1:600 dilution; ThermoFisher, 49-1012) at 4 °C in a humidified chamber. Alexa Fluor 488 conjugated anti-mouse and anti-rabbit IgG (1:400 dilution; Invitrogen, A-11001 and A32731) were used as secondary antibodies to visualize immunosignals. Sections were counterstained in 1 µg ml^{-1} PI, rinsed in water and imaged with an A1R laser scanning confocal microscope (Nikon) (AF488, excitation 488 nm, emission 505–520 nm; PI, excitation 561 nm, emission 590–640 nm). The primary antibodies were omitted for the negative control. Antibody and PI signals were measured using ImageJ.

Phylogenetic analysis

A phylogenetic tree was reconstructed with aligned full-length amino acid sequences of homologues of MADS31. Evolutionary history was inferred using the neighbour-joining method. The evolutionary distances were computed using the Poisson correction method and are in units of 'number of amino acid substitutions per site'. This

analysis involved 10 amino acid sequences. All ambiguous positions were removed for each sequence pair (pairwise deletion option). Evolutionary analyses were conducted in MEGA11 (ref. 103).

Statistical analysis and replication

For all cytological analysis in ovules, including measurement of embryo sac area, resin sections and pectin immunolabelling, 50–100 spikelets (for observation of young ovules) or pistils (for observation of mature ovules) were collected from 4–6 barley and wheat plants of various genotypes and fixed in FAA. A certain number of spikelets or pistils were randomly picked for various experiments; the exact numbers of ovules used for cellular morphology and fluorescence intensity measurement are shown in figures or figure legends. If not specified, at least 3 ovules were observed, and representative images are shown in figures.

For experiments using paraffin sections, including in situ hybridization, TUNEL assay and histone methylation immunolabelling, 50–100 spikelets or pistils were collected from 4–6 replicate barley plants of each genotype and fixed in FAA[39]. At least 20 spikelets or pistils for each genotype were randomly picked and embedded in paraffin. Experiments were performed 3 times using >3 samples for each repeat. All technical replicates showed similar results and representative images are shown in figures.

For RNA extraction and ChIP experiments, 200–1,000-mg spikelets or pistils were collected from 4–6 barley plants of various genotypes, except that samples were collected from each plant of *NRPD4b* overexpression lines. For RT–qPCR and ChIP–PCR, at least 3 technical replicates were performed.

For dual-LUC, a whole tobacco leaf was infiltrated with *A. tumefaciens* culture. A puncher with 5-mm diameter was used to collect 5–8 pieces of samples as replicates for luciferase activity assay.

For eGFP signal observation in transgenic lines, at least 3 ovules were examined from each of 3 plants. Representative images are shown in figures.

For seed set percentages, 4–9 barley or wheat plants of various genotypes were used as biological replicates, as indicated in figures or figure legends. In the case of *NRPD4b* overexpression lines, 4 spikes from each plant were used as biological replicates.

GraphPad Prism 9 and Microsoft Excel 2016 were used for statistical analyses and generating graphs. Statistical methods used are described in figure legends and exact *P* values are shown in figures.

Reporting summary

Further information on research design is available in the Nature Portfolio Reporting Summary linked to this article.

Data availability

The RNA-seq data generated in this study have been deposited to the NCBI database under project accession number SRA: PRJNA1187641. Additional data, such as raw image files, that are relevant to the findings of this study are available from the corresponding author upon request. The Morex V1 genome is available at http://webblast.ipk-gatersleben.de. The Morex V3 genome is available at https://plants.ensembl.org/Hordeum_vulgare/Info/Index. The barley transposable elements are available at https://wheat.pw.usda.gov/GG3/content/morex-v3-files-2021. Source data are provided with this paper.

References

1. Rudall, P. J. Evolution and patterning of the ovule in seed plants. *Biol. Rev.* **96**, 943–960 (2021).
2. Lora, J., Yang, X. & Tucker, M. R. Establishing a framework for female germline initiation in the plant ovule. *J. Exp. Bot.* **70**, 2937–2949 (2019).
3. Shi, D. Q. & Yang, W. C. Ovule development in *Arabidopsis*: progress and challenge. *Curr. Opin. Plant Biol.* **14**, 74–80 (2011).
4. Drews, G. N. & Koltunow, A. M. in *The Arabidopsis Book* https://doi.org/10.1199/tab.0155 (BioOne, 2011).
5. Endress, P. K. Angiosperm ovules: diversity, development, evolution. *Ann. Bot.* **107**, 1465–1489 (2011).
6. Pinto, S. C. et al. Revisiting the female germline and its expanding toolbox. *Trends Plant Sci.* **24**, 455–467 (2019).
7. Schiefthaler, U. et al. Molecular analysis of *NOZZLE*, a gene involved in pattern formation and early sporogenesis during sex organ development in *Arabidopsis thaliana*. *Proc. Natl Acad. Sci. USA* **96**, 11664–11669 (1999).
8. Yang, W. C. et al. The *SPOROCYTELESS* gene of *Arabidopsis* is required for initiation of sporogenesis and encodes a novel nuclear protein. *Genes Dev.* **13**, 2108–2117 (1999).
9. Garcia-Aguilar, M. et al. Inactivation of a DNA methylation pathway in maize reproductive organs results in apomixis-like phenotypes. *Plant Cell* **22**, 3249–3267 (2010).
10. Olmedo-Monfil, V. et al. Control of female gamete formation by a small RNA pathway in *Arabidopsis*. *Nature* **464**, 628–632 (2010).
11. Nonomura, K. I. et al. The MSP1 gene is necessary to restrict the number of cells entering into male and female sporogenesis and to initiate anther wall formation in rice. *Plant Cell* **15**, 1728–1739 (2003).
12. Cheng, C. Y. et al. Cytokinin-dependent specification of the functional megaspore in the *Arabidopsis* female gametophyte. *Plant J.* **73**, 929–940 (2013).
13. Ceccato, L. et al. Maternal control of PIN1 is required for female gametophyte development in *Arabidopsis*. *PLoS ONE* **8**, e66148 (2013).
14. Rojek, J. et al. The Rab geranylgeranyl transferase beta subunit is essential for embryo and seed development in *Arabidopsis thaliana*. *Int. J. Mol. Sci.* **22**, 7907 (2021).
15. Mendes, M. A. et al. The RNA-dependent DNA methylation pathway is required to restrict *SPOROCYTELESS/NOZZLE* expression to specify a single female germ cell precursor in *Arabidopsis*. *Development* **147**, dev194274 (2020).
16. Wang, J. et al. Auxin efflux controls orderly nucellar degeneration and expansion of the female gametophyte in *Arabidopsis*. *New Phytol.* **230**, 2261–2274 (2021).
17. Radchuk, V. et al. *Jekyll* encodes a novel protein involved in the sexual reproduction of barley. *Plant Cell* **18**, 1652–1666 (2006).
18. Radchuk, V. et al. Grain filling in barley relies on developmentally controlled programmed cell death. *Commun. Biol.* **4**, 428 (2021).
19. Daneva, A. et al. Functions and regulation of programmed cell death in plant development. *Annu. Rev. Cell Dev. Biol.* **32**, 441–468 (2016).
20. Wang, Y. et al. The regulatory framework of developmentally programmed cell death in floral organs: a review. *Plant Physiol. Biochem.* **158**, 103–112 (2021).
21. Yin, L. L. & Xue, H. W. The MADS29 transcription factor regulates the degradation of the nucellus and the nucellar projection during rice seed development. *Plant Cell* **24**, 1049–1065 (2012).
22. Shoesmith, J. R. et al. APETALA2 functions as a temporal factor together with BLADE-ON-PETIOLE2 and MADS29 to control flower and grain development in barley. *Development* **148**, 194894 (2021).
23. Liu, G. et al. TaMADS29 interacts with TaNF-YB1 to synergistically regulate early grain development in bread wheat. *Sci. China Life Sci.* **66**, 1647–1664 (2023).
24. Favaro, R. et al. MADS-box protein complexes control carpel and ovule development in *Arabidopsis*. *Plant Cell* **15**, 2603–2611 (2003).
25. Pinyopich, A. et al. Assessing the redundancy of MADS-box genes during carpel and ovule development. *Nature* **424**, 85–88 (2003).
26. Brambilla, V. et al. Genetic and molecular interactions between BELL1 and MADS box factors support ovule development in *Arabidopsis*. *Plant Cell* **19**, 2544–2556 (2007).

27. Becker, A. et al. A novel MADS-box gene subfamily with a sister-group relationship to class B floral homeotic genes. *Mol. Genet. Genomics* **266**, 942–950 (2002).
28. Frohlich, M. W.An evolutionary scenario for the origin of flowers. *Nat. Rev. Genet.* **4**, 559–566 (2003).
29. Xu, W. et al. Endosperm and nucellus develop antagonistically in *Arabidopsis* seeds. *Plant Cell* **28**, 1343–1360 (2016).
30. Mizzotti, C. et al. The MADS box genes *SEEDSTICK* and *ARABIDOPSIS Bsister* play a maternal role in fertilization and seed development. *Plant J.* **70**, 409–420 (2012).
31. Nesi, N. et al. The *TRANSPARENT TESTA16* locus encodes the ARABIDOPSIS BSISTER MADS domain protein and is required for proper development and pigmentation of the seed coat. *Plant Cell* **14**, 2463–2479 (2002).
32. Prasad, K. et al. The *Arabidopsis* B-sister MADS-box protein, GORDITA, represses fruit growth and contributes to integument development. *Plant J.* **62**, 203–214 (2010).
33. Erdmann, R. et al. *GORDITA (AGL63)* is a young paralog of the *Arabidopsis thaliana* Bsister MADS box gene *ABS (TT16)* that has undergone neofunctionalization. *Plant J.* **63**, 914–924 (2010).
34. Shen, C. Y. et al. Orchid Bsister gene *PeMADS28* displays conserved function in ovule integument development. *Sci. Rep.* **11**, 1205 (2021).
35. Yang, X. et al. Live and let die - the Bsister MADS-box gene *OsMADS29* controls the degeneration of cells in maternal tissues during seed development of rice (*Oryza sativa*). *PLoS ONE* **7**, e51435 (2012).
36. Lee, D. S. et al. The Bsister MADS gene *FST* determines ovule patterning and development of the zygotic embryo and endosperm. *PLoS ONE* **8**, e58748 (2013).
37. Schilling, S. et al. Non-canonical structure, function and phylogeny of the B sister MADS-box gene *OsMADS30* of rice (*Oryza sativa*). *Plant J.* **84**, 1059–1072 (2015).
38. Wilkinson, L. G. Molecular and genetic cues influencing ovule development in barley (*Hordeum vulgare* L.). PhD thesis, University of Adelaide (2019).
39. Yang, X. et al. Ovule cell wall composition is a maternal determinant of grain size in barley. *New Phytol.* **237**, 2136–2147 (2023).
40. Wilkinson, L. G. et al. Natural variation in ovule morphology is influenced by multiple tissues and impacts downstream grain development in barley (*Hordeum vulgare L.*). *Front. Plant Sci.* **10**, 1374 (2019).
41. Ma, X. et al. A robust CRISPR/Cas9 system for convenient, high-efficiency multiplex genome editing in monocot and dicot plants. *Mol. Plant* **8**, 1274–1284 (2015).
42. Chen, X. & Rechavi, O. Plant and animal small RNA communications between cells and organisms. *Nat. Rev. Mol. Cell Biol.* **23**, 185–203 (2022).
43. Hara-Nishimura, I. & Hatsugai, N.The role of vacuole in plant cell death. *Cell Death Differ.* **18**, 1298–1304 (2011).
44. Jiang, J. et al. WRKY transcription factors in plant responses to stresses. *J. Integr. Plant Biol.* **59**, 86–101 (2017).
45. Zhou, J. M. & Zhang, Y. Plant immunity: danger perception and signaling. *Cell* **181**, 978–989 (2020).
46. Gramzow, L. & Theissen, G. A hitchhiker's guide to the MADS world of plants. *Genome Biol.* **11**, 214 (2010).
47. Aubert, M. K. Molecular and genetic characterisation of early aleurone development in barley (*Hordeum vulgare* L.). PhD thesis, University of Adelaide (2018).
48. Waddington, S. R., Cartwright, P. M. & Wall, P. C. A quantitative scale of spike initial and pistil development in barley and wheat. *Ann. Bot.* **51**, 119–130 (1983).
49. Wei, L. et al. Dicer-like 3 produces transposable element-associated 24-nt siRNAs that control agricultural traits in rice. *Proc. Natl Acad. Sci. USA* **111**, 3877–3882 (2014).
50. Xu, L. et al. Regulation of rice tillering by RNA-directed DNA methylation at miniature inverted-repeat transposable elements. *Mol. Plant* **13**, 851–863 (2020).
51. Singh, M. et al. Production of viable gametes without meiosis in maize deficient for an ARGONAUTE protein. *Plant Cell* **23**, 443–458 (2011).
52. He, X. J. et al. NRPD4, a protein related to the RPB4 subunit of RNA polymerase II, is a component of RNA polymerases IV and V and is required for RNA-directed DNA methylation. *Genes Dev.* **23**, 318–330 (2009).
53. Baroux, C., Pien, S. & Grossniklaus, U. Chromatin modification and remodeling during early seed development. *Curr. Opin. Genet. Dev.* **17**, 473–479 (2007).
54. Huanca-Mamani, W. et al. CHR11, a chromatin-remodeling factor essential for nuclear proliferation during female gametogenesis in *Arabidopsis thaliana*. *Proc. Natl Acad. Sci. USA* **102**, 17231–17236 (2005).
55. Cai, H. et al. Spatiotemporal control of miR398 biogenesis, via chromatin remodeling and kinase signaling, ensures proper ovule development. *Plant Cell* **33**, 1530–1553 (2021).
56. She, W. et al. Chromatin reprogramming during the somatic-to-reproductive cell fate transition in plants. *Development* **140**, 4008–4019 (2013).
57. Oliver, C. et al. The dynamics of histone H3 modifications is species-specific in plant meiosis. *Planta* **238**, 23–33 (2013).
58. Aditya, J. et al. The dynamics of cereal cyst nematode infection differ between susceptible and resistant barley cultivars and lead to changes in (1, 3; 1, 4)-β-glucan levels and HvCslF gene transcript abundance. *New Phytol.* **207**, 135–147 (2015).
59. Pinto, S. C. et al. Germline β–1,3-glucan deposits are required for female gametogenesis in *Arabidopsis thaliana*. *Nat. Commun.* **15**, 5875 (2024).
60. Drews, G. N., Lee, D. & Christensen, C. A. Genetic analysis of female gametophyte development and function. *Plant Cell* **10**, 5–17 (1998).
61. Bencivenga, S., Colombo, L. & Masiero, S. Cross talk between the sporophyte and the megagametophyte during ovule development. *Sex. Plant Reprod.* **24**, 113–121 (2011).
62. Lu, J. & Magnani, E. Seed tissue and nutrient partitioning, a case for the nucellus. *Plant Reprod.* **31**, 309–317 (2018).
63. Dominguez, F., Moreno, J. & Cejudo, F. J. The nucellus degenerates by a process of programmed cell death during the early stages of wheat grain development. *Planta* **213**, 352–360 (2001).
64. Li, C. et al. Single-nucleus sequencing deciphers developmental trajectories in rice pistils. *Dev. Cell* **58**, 694–708 (2023).
65. Folsom, M. W. & Cass, D. D. The characteristics and fate of the soybean inner nucellus. *Acta Bot. Neerl.* **37**, 387–393 (1988).
66. Douglas, A. W., Stevenson, D. W. & Little, D. P. Ovule development in *Ginkgo biloba* L., with emphasis on the collar and nucellus. *Int. J. Plant Sci.* **168**, 1207–1236 (2007).
67. Lu, J. et al. The nucellus: between cell elimination and sugar transport. *Plant Physiol.* **185**, 478–490 (2021).
68. Russell, S. D. Fine structure of megagametophyte development in *Zea mays*. *Can. J. Bot.* **57**, 1093–1110 (1979).
69. Nogueira, F. M. et al. Ultrastructural analysis of *Rhynchospora* ovules: the first record of Cyperaceae megagametophyte on transmission electron microscope. *Micron* **140**, 02962 (2021).
70. Parish, R. W. & Li, S. F. Death of a tapetum: a programme of developmental altruism. *Plant Sci.* **178**, 73–89 (2010).
71. Marchant, D. B. & Walbot, V. Anther development—the long road to making pollen. *Plant Cell* **34**, 4677–4695 (2022).
72. Long, J. et al. Nurse cell-derived small RNAs define paternal epigenetic inheritance in *Arabidopsis*. *Science* **373**, eabh0556 (2021).

73. Rodríguez-Leal, D. et al. Natural variation in epigenetic pathways affects the specification of female gamete precursors in *Arabidopsis*. *Plant Cell* **27**, 1034–1045 (2015).
74. Su, Z. et al. Regulation of female germline specification via small RNA mobility in *Arabidopsis*. *Plant Cell* **32**, 2842–2854 (2020).
75. Grini, P. E. et al. The ASH1 HOMOLOG 2 (ASHH2) histone H3 methyltransferase is required for ovule and anther development in *Arabidopsis*. *PLoS ONE* **4**, e7817 (2009).
76. Lv, Y. et al. Polycomb proteins RING1A/B promote H2A monoubiquitination to regulate female gametophyte development in *Arabidopsis*. *J. Exp. Bot.* **75**, 4822–4836 (2024).
77. Huang, Y. et al. Epigenetic regulation of female germline development through ERECTA signaling pathway. *New Phytol.* **240**, 1015–1033 (2023).
78. Yang, F. et al. Characterization and functional analysis of a MADS-box transcription factor gene (*GbMADS9*) from *Ginkgo biloba*. *Sci. Hortic.* **212**, 104–114 (2016).
79. Hu, J. et al. The pineapple MADS-box gene family and the evolution of early monocot flower. *Sci. Rep.* **11**, 849 (2021).
80. de Folter, S. et al. A Bsister MADS-box gene involved in ovule and seed development in petunia and *Arabidopsis*. *Plant J.* **47**, 934–946 (2006).
81. Nayar, S. et al. Functional delineation of rice MADS29 reveals its role in embryo and endosperm development by affecting hormone homeostasis. *J. Exp. Bot.* **64**, 4239–4253 (2013).
82. Ng, M. & Yanofsky, M. F. Function and evolution of the plant MADS-box gene family. *Nat. Rev. Genet.* **2**, 186–195 (2001).
83. Nayar, S., Kapoor, M. & Kapoor, S. Post-translational regulation of rice MADS29 function: homodimerization or binary interactions with other seed-expressed MADS proteins modulate its translocation into the nucleus. *J. Exp. Bot.* **65**, 5339–5350 (2014).
84. Masiero, S. et al. Ternary complex formation between MADS-box transcription factors and the histone fold protein NF-YB. *J. Biol. Chem.* **277**, 26429–26435 (2002).
85. Abraham-Juárez, M. J. et al. Evolutionary variation in MADS box dimerization affects floral development and protein abundance in maize. *Plant Cell* **32**, 3408–3424 (2020).
86. Lai, X. et al. The LEAFY floral regulator displays pioneer transcription factor properties. *Mol. Plant* **14**, 829–837 (2021).
87. Bartlett, J. G. et al. High-throughput *Agrobacterium*-mediated barley transformation. *Plant Methods* **4**, 22 (2008).
88. Naito, Y. et al. CRISPRdirect: software for designing CRISPR/Cas guide RNA with reduced off-target sites. *Bioinformatics* **31**, 1120–1123 (2015).
89. He, Y. et al. A phase-separated protein hub modulates resistance to *Fusarium* head blight in wheat. *Cell Host Microbe* **32**, 710–726 (2024).
90. Ishida, Y. et al. Wheat (*Triticum aestivum* L.) transformation using immature embryos. *Methods Mol. Biol.* **1223**, 189–198 (2015).
91. Wilkinson, L. G. & Tucker, M. R. An optimised clearing protocol for the quantitative assessment of sub-epidermal ovule tissues within whole cereal pistils. *Plant Methods* **13**, 67 (2017).
92. Betts, N. S. et al. Morphology, carbohydrate distribution, gene expression, and enzymatic activities related to cell wall hydrolysis in four barley varieties during simulated malting. *Front. Plant Sci.* **8**, 1872 (2017).
93. Mascher, M. et al. A chromosome conformation capture ordered sequence of the barley genome. *Nature* **544**, 427–433 (2017).
94. Yu, G. et al. clusterProfiler: an R package for comparing biological themes among gene clusters. *OMICS* **16**, 284–287 (2012).
95. Metsalu, T. & Vilo, J. ClustVis: a web tool for visualizing clustering of multivariate data using Principal Component Analysis and heatmap. *Nucleic Acids Res.* **43**, 566–570 (2015).
96. Chen, S. et al. fastp: an ultra-fast all-in-one FASTQ preprocessor. *Bioinformatics* **34**, 884–890 (2018).
97. Langmead, B. et al. Ultrafast and memory-efficient alignment of short DNA sequences to the human genome. *Genome Biol.* **10**, R25 (2009).
98. Quinlan, A. R. & Hall, I. M. BEDTools: a flexible suite of utilities for comparing genomic features. *Bioinformatics* **26**, 841–842 (2010).
99. Ramírez, F. et al. deepTools: a flexible platform for exploring deep-sequencing data. *Nucleic Acids Res.* **42**, 187–191 (2014).
100. Li, G. et al. MADS1 maintains barley spike morphology at high ambient temperatures. *Nat. Plants* **7**, 1093–1107 (2021).
101. Dasgupta, P. & Chaudhuri, S. Analysis of DNA methylation profile in plants by Chop-PCR. *Methods Mol. Biol.* **1991**, 79–90 (2019).
102. Nic-Can, G. et al. An efficient immunodetection method for histone modifications in plants. *Plant Methods* **9**, 47 (2013).
103. Tamura, K., Stecher, G. & Kumar, S. MEGA11: molecular evolutionary genetics analysis version 11. *Mol. Biol. Evol.* **38**, 3022–3027 (2021).

Acknowledgements

We thank C. Ma and S. Johnson for technical assistance; A. Koltunow, T. Laux, M. Mendes, S. Pinto, D. Yang and D. Xu for productive discussions. LCM experiments and microscopy work were undertaken with support from G. Mayo at Adelaide Microscopy, and plants were grown in The Plant Accelerator, an Australian NCRIS-funded facility. This research was supported by Australian Research Council grants DP180104092, DP210103491, IC210100047 and CE230100015. K.H. acknowledges funding from the Rural and Environment Science and Analytical Services Division of the Scottish Government. The authors acknowledge D. Cakouros and T. Bianco-Miotto (University of Adelaide) for advising on histone methylation immunolabelling, D. Peet (University of Adelaide) for assistance with dual-luciferase assays and Y. Liu (South China Agricultural University) for providing vectors pYLsgRNA–OsU6a, pYLsgRNA–OsU6b and pYLCRISPR–Cas9Pubi–H for CRISPR/Cas9 editing. The authors acknowledge the instruments and expertise of Microscopy Australia (ROR: 042mm0k03) at Adelaide Microscopy, University of Adelaide, enabled by NCRIS, university and state government support.

Author contributions

X.Y. and M.R.T. designed the study. X.Y. and G.L. were responsible for phenotyping, generating transgenic plants, molecular biology and microscopy experiments. L.G.W. and M.K.A. collected and generated LCM data. J.S. and N.J.S. analysed transcriptomic data. H.G. analysed small RNA sequencing data. K.H., L.C. and R.L. contributed to data analysis and discussion. X.Y. and M.R.T. wrote the manuscript. All authors contributed to the editing and reviewing of the manuscript.

Competing interests

The authors declare no competing interests.

Additional information

Extended data is available for this paper at https://doi.org/10.1038/s41477-025-01915-z.

Supplementary information The online version contains supplementary material available at https://doi.org/10.1038/s41477-025-01915-z.

Correspondence and requests for materials should be addressed to Matthew R. Tucker.

Peer review information *Nature Plants* thanks Volodymyr Radchuk and the other, anonymous, reviewer(s) for their contribution to the peer review of this work.

Xiujuan Yang[1], Gang Li[1,2], Jin Shi[3], Laura G. Wilkinson[1], Matthew K. Aubert[1,9], Kelly Houston[4], Neil J. Shirley[1], Hengbin Gao[5], Ryan Lister[5], Lucia Colombo[6] & Matthew R. Tucker[1,7,8] ✉

[1]Waite Research Institute, School of Agriculture, Food and Wine, The University of Adelaide, Urrbrae, South Australia, Australia. [2]State Key Laboratory of Agricultural and Forestry Biosecurity, College of Plant Protection, Nanjing Agricultural University, Nanjing, China. [3]School of Life Sciences and Biotechnology, Shanghai Jiao Tong University, Shanghai, China. [4]The James Hutton Institute, Invergowrie, Dundee, Scotland, UK. [5]The Harry Perkins Institute of Medical Research, QEII Medical Centre and Centre for Medical Research, The University of Western Australia, Perth, Western Australia, Australia. [6]Department of Biosciences, Università degli Studi di Milano, Milan, Italy. [7]ARC Centre of Excellence in Plants for Space, The University of Adelaide, Urrbrae, South Australia, Australia. [8]ARC Training Centre for Future Crops Development, The University of Adelaide, Urrbrae, South Australia, Australia. [9]Present address: Australian Grain Technologies, Northam, Western Australia, Australia. ✉e-mail: matthew.tucker@adelaide.edu.au

https://doi.org/10.1038/s41477-025-01915-z

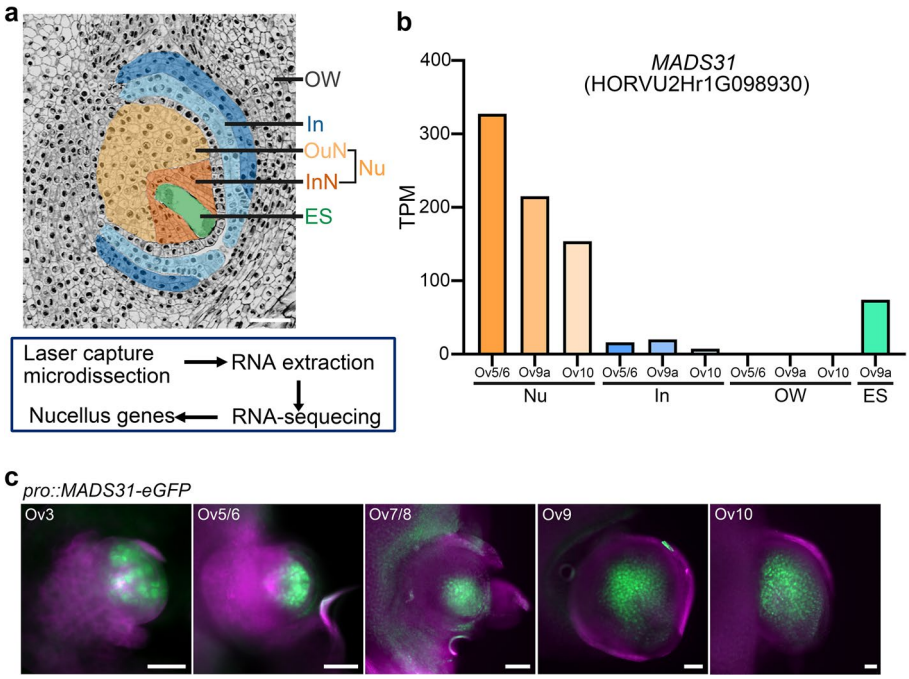

Extended Data Fig. 1 | Spatial and temporal expression pattern of *MADS31*. **a**, The procedure of tissue-specific transcriptome profiling. OW, ovary wall; In, integuments; OuN, outer nucellus; InN, inner nucellus; Nu, nucellus; ES, embryo sac/female gametophyte. Scale bar, 50 μm. **b**, *MADS31* expression in ovule tissues by RNA-sequencing. TPM, transcripts per million. Ov5/6, female gametophyte (FG) mitosis stage; Ov9a, mature FG stage; Ov10, FG at anthesis stage. Gradients of column color indicate different development stages. **c**, Accumulation of MADS31 protein during ovule development in *pro::MADS31-eGFP* transgenic lines. The UV channel is used as background emission shown in magenta. Scale bars, 50 μm. Observations were repeated three times in three independent transgenic lines with similar results.

https://doi.org/10.1038/s41477-025-01915-z

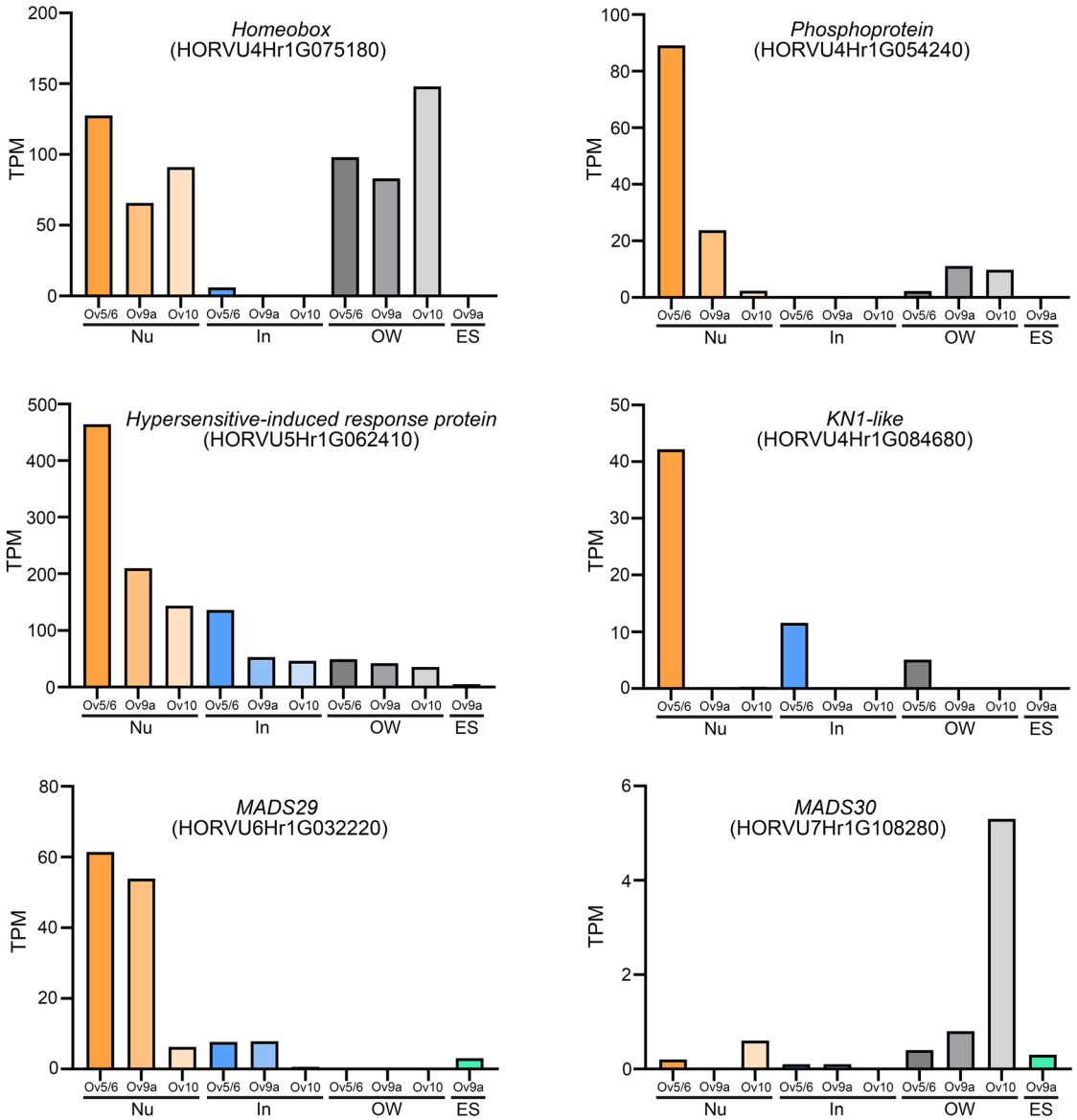

Extended Data Fig. 2 | Examples of genes expressed in the nucellus of the barley ovule. *KN1, KNOTTED1*. In addition to *MADS31*, *MADS29* and *MADS30* are the other two members of the B-sister class of MADS box genes in barley. Gradients of column colour indicate different developmental stages.

https://doi.org/10.1038/s41477-025-01915-z

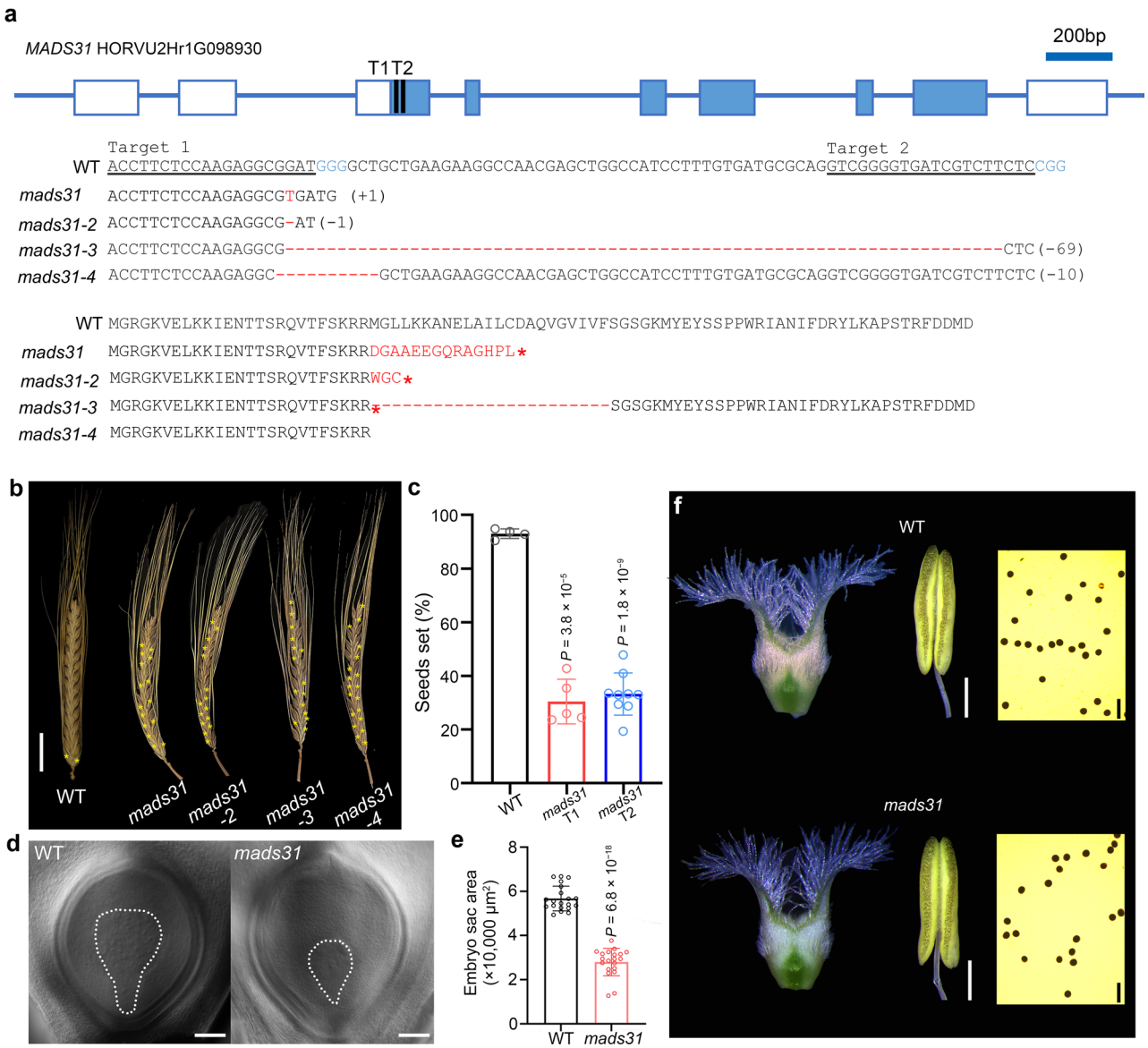

Extended Data Fig. 3 | Creation of barley *mads31* mutants using CRISPR/Cas9. a, Upper, the gene structure of *MADS31* and the positions of two sgRNA targets (T1 and T2) for gene editing. Blue boxes are exons and white boxes are UTRs. Middle, DNA sequences of mutations in *MADS31*. Lower, putative amino acid sequences in *mads31* mutants. Asterisks indicate a stop codon. WT, wild type. **b**, Mature spikes of WT and four alleles of *mads31*. Yellow asterisks indicate sterile spikelets. Scale bars, 2 cm. **c**, Seed set rate of WT and *mads31* (T1 and T2 generation transgenic lines). The data are shown as mean ± s.d.; 4, 5 and 9 individual plants are used for each genotype; *t*-test for unpaired two-sample data, two-sided. **d**, Ovules from cleared pistils in WT and *mads31*. White dashed lines indicate embryo sacs. Scale bars, 100 μm. **e**, Measurement of embryo sac area from cleared pistils. The data are shown as mean ± s.d.; $n = 20$ replicates; *t*-test, two-sided. **f**, Pistils and anthers of WT and *mads31*. Left, pistils at anthesis. Middle, anthers at anthesis. Scale bars, 1 mm. Right, pollen stained by I_2-KI solution. Scale bars, 100 μm.

https://doi.org/10.1038/s41477-025-01915-z

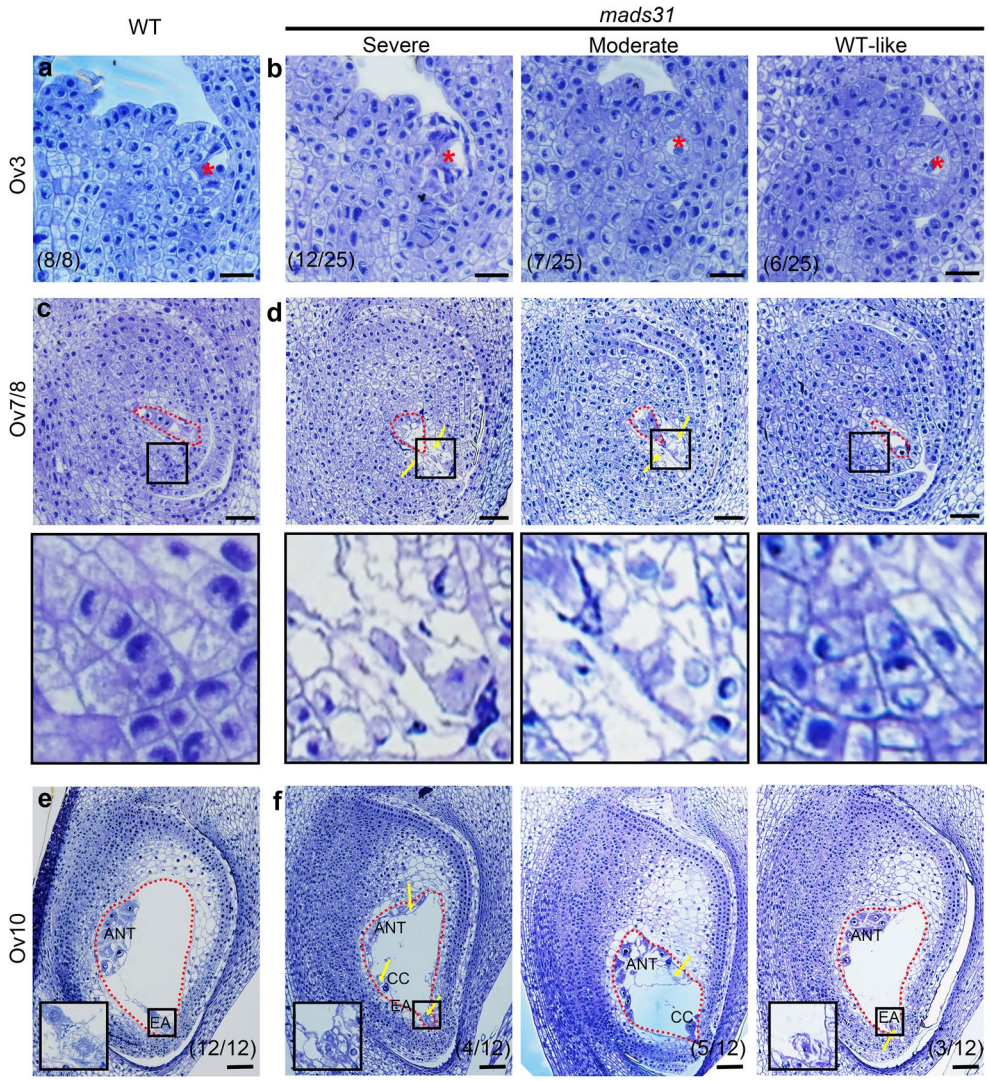

Extended Data Fig. 4 | Morphological changes in the inner nucellus and germline in *mads31*. a, b, Longitudinal sections of wild-type (WT) and *mads31* ovules at Ov3 stage. Red asterisks indicate the megaspore mother cell. Scale bars, 25 μm. **c, d**, Longitudinal sections of WT and *mads31* ovules at Ov7/8 stage. Red dashed lines indicate the embryo sac. Black squares are enlarged to highlight differences in the inner nucellus. Scale bars, 50 μm. **e, f**, Longitudinal sections of WT and *mads31* ovules at Ov10 stage. Altered nucellus morphology can be seen in all mutants, including "WT-like" *mads31* mutants. Red dashed lines indicate the embryo sac. Yellow arrows indicate cell vacuolation. Black squares are enlargement of the egg apparatus. ANT, antipodal cells; CC, central cell; EA, egg apparatus. Numbers in parentheses in **f** indicate the number of mutant ovules identified in each category. Scale bars, 50 μm. Representative images were shown from sections of certain number of ovules (in black bracket of a, b, e and **f**, 3 ovules for **c** and **d**).

https://doi.org/10.1038/s41477-025-01915-z

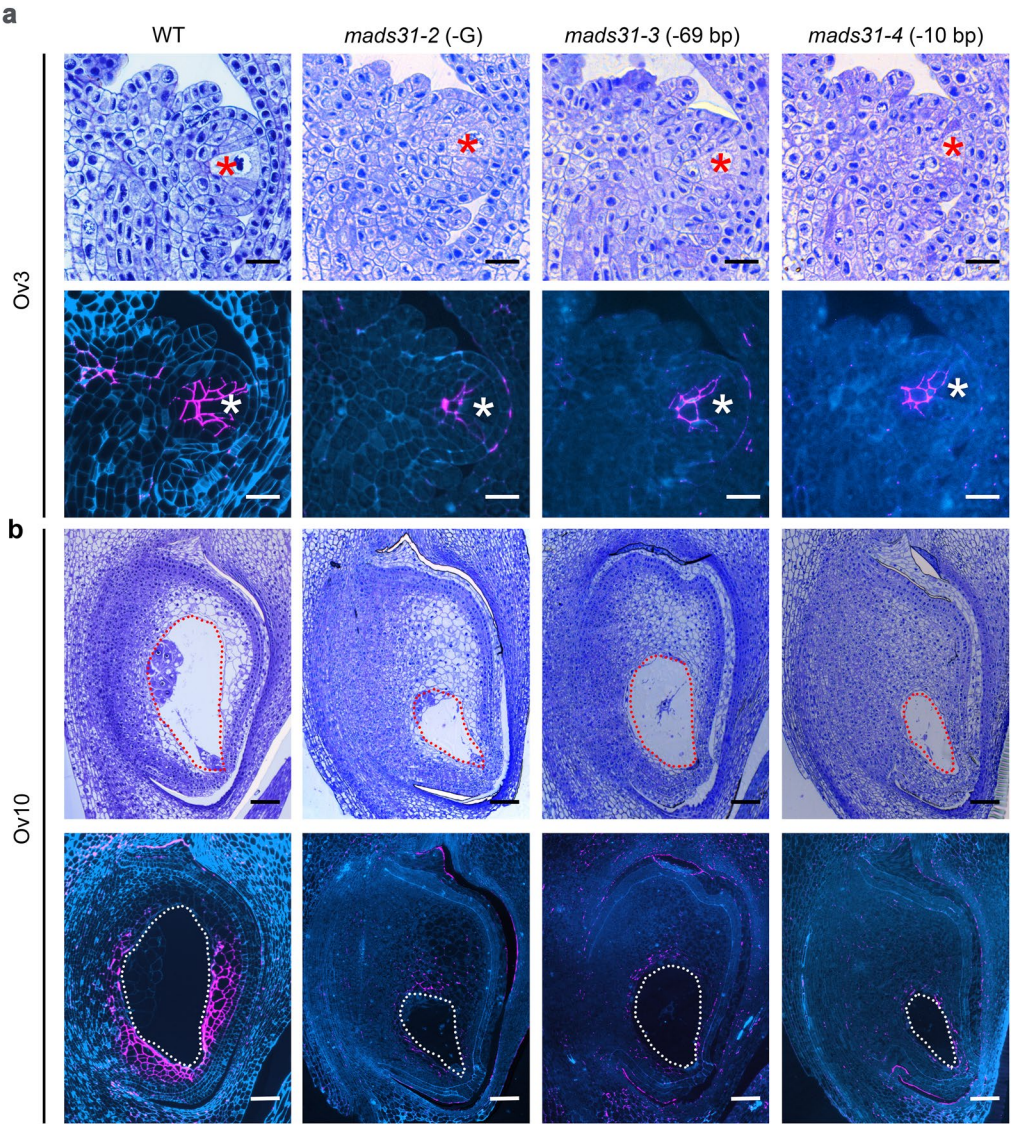

Extended Data Fig. 5 | Inner nucellus phenotypes in *mads31* alleles. a, Longitudinal sections (upper) and LM19 immunolabeling (lower) of wild-type (WT) and *mads31-2/-3/-4* ovules at Ov3 stage. Red and white asterisks indicate the megaspore mother cell. Scale bars, 25 µm. **b**, Longitudinal sections (upper) and LM19 immunolabeling (lower) of WT and *mads31-2/-3/-4* ovules at Ov10 stage. Red and white dashed lines indicate the embryo sac. Scale bars, 50 µm. Representative images were shown from sections of 3 ovules for each stage and each genotype.

https://doi.org/10.1038/s41477-025-01915-z

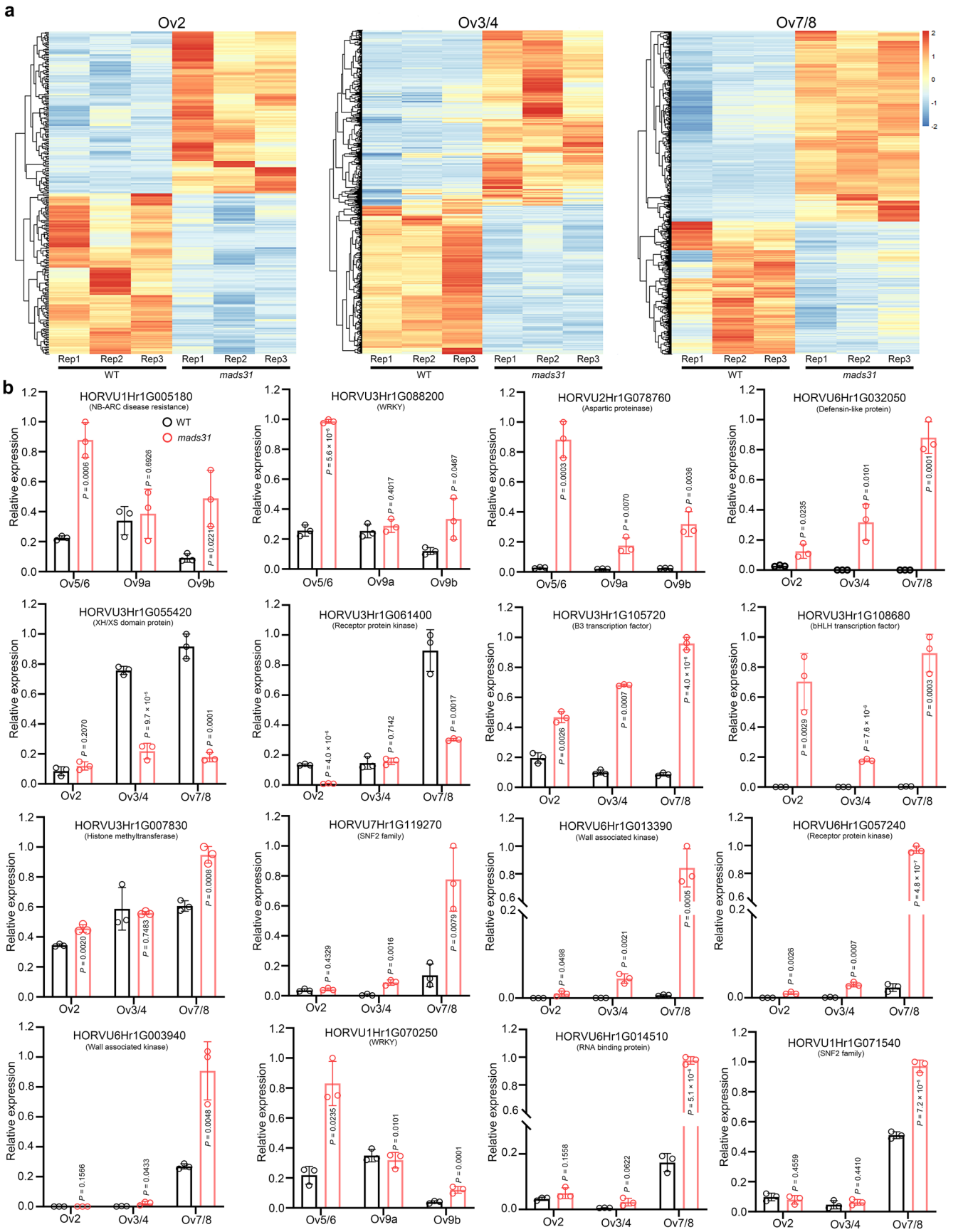

Extended Data Fig. 6 | Transcriptome profiling and verification of DEGs in *mads31*. **a**, Overview of differentially expressed genes (DEGs) between wild type (WT) and *mads31* at Ov2, Ov3, and Ov7/8 stages. **b**, Verifying expression change by qRT-PCR. The data are shown as mean ± s.d.; $n = 3$ replicates; *t*-test, two-sided.

https://doi.org/10.1038/s41477-025-01915-z

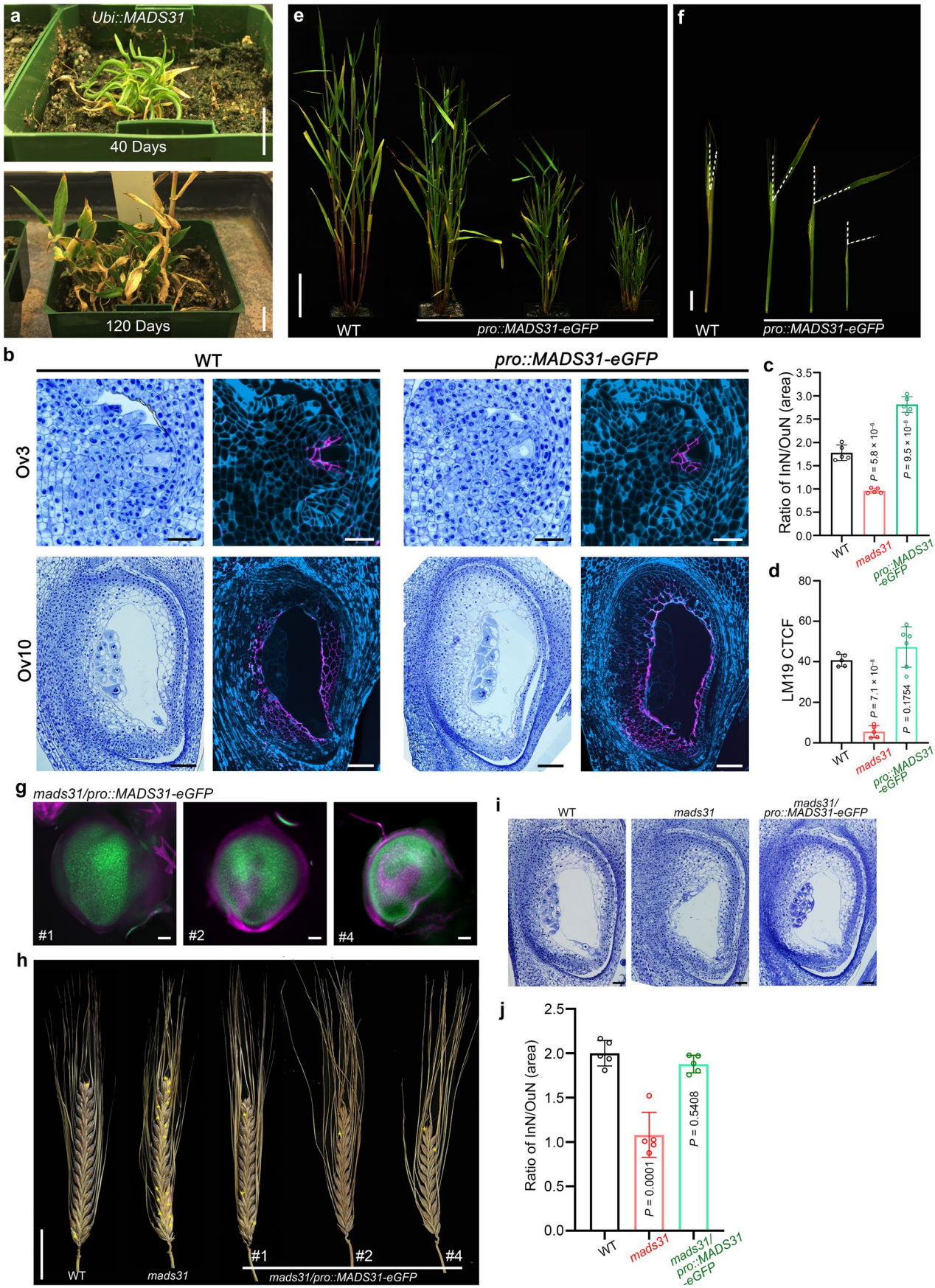

Extended Data Fig. 7 | See next page for caption.

https://doi.org/10.1038/s41477-025-01915-z

Extended Data Fig. 7 | Fusion of MADS31 to eGFP can function in plants. a, Extreme dwarfism in *Ubi::MADS31* transgenic plants. 40 days and 120 days indicate growth time after plants were transferred to soil. Scale bars, 1 cm. **b**, Nucellus patterning in wild-type (WT) and *pro::MADS31-eGFP* ovules. Left, toluidine blue stained longitudinal sections. Right, LM19 labelled demethylesterified pectin in the cell walls of nucellus. Scale bars, 25 μm (Ov3) and 100 μm (Ov10). **c**, Ratios of inner nucellus area versus outer nucellus area in WT, *mads31* and *pro::MADS31-eGFP* ovules. **d**, Corrected total cell fluorescence (CTCF) of LM19 immunosignals in the nucellus of WT, *mads31* and *pro::MADS31-eGFP* ovules. **e**, Various degrees of dwarfism in *pro::MADS31-eGFP* transgenic plants. Scale bar, 10 cm. **f**, Flag leaf inclination in wild-type (WT) and *pro::MADS31-eGFP* plants. Scale bar, 2 cm. **g**, Expression of MADS31-eGFP fusion protein in three transgenic *mads31* plants. Scale bars, 100 μm. **h**, Mature spikes of WT, *mads31* and *mads31/pro::MADS31-eGFP* plants. Yellow asterisks indicate sterile spikelets. Scale bar, 2 cm. **i**, Longitudinal sections of wild-type (WT), *mads31* and *mads31/pro::MADS31-eGFP* ovules. Scale bars, 50 μm. **j**, Ratios of inner nucellus area versus outer nucellus area in WT, *mads31* and mads31/*pro::MADS31-eGFP* ovules. In **c**, **d** and **j**, the data are shown as mean ± s.d.; $n = 5$ ovules; *t*-test for unpaired two-sample data, two-sided.

https://doi.org/10.1038/s41477-025-01915-z

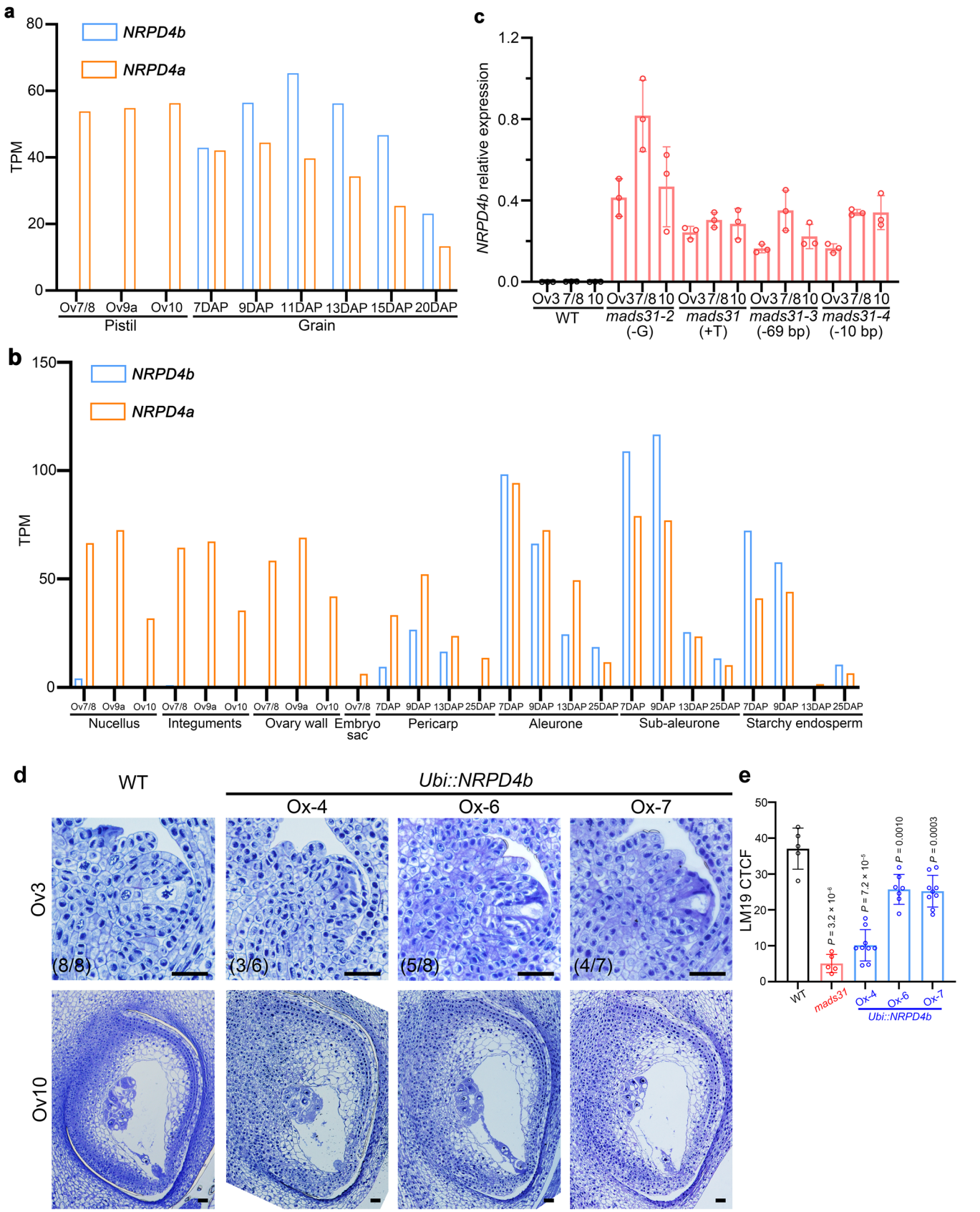

Extended Data Fig. 8 | See next page for caption.

https://doi.org/10.1038/s41477-025-01915-z

Extended Data Fig. 8 | Expression patterns of *NRPD4a* and *NRPD4b* and overexpression of *NRPD4b* causes nucellus patterning defects. a, *NRPD4a and NRPD4b* expression in pistils and grains. **b**, *NRPD4a and NRPD4b* expression levels in various tissues of the pistil and grain. DAP, days after pollination. TPM, transcripts per million. **c**, Relative expression level (RT-qPCR) of *NRPD4b* in WT and *mads31* alleles. The data are shown as mean ± s.d.; $n = 3$ replicates. **d**, Longitudinal sections of wild-type (WT) and *Ubi::NRPD4b* ovules at Ov3 and Ov10 stages. Defects in *Ubi::NRPD4b* are already observed at stage Ov3 including abnormal inner nucellus cell morphology. At Ov10 stage, Ox lines show an increased abundance of outer nucellus cells and variable cell shape and morphology in the inner nucellus. Numbers in parentheses indicate frequencies of defective ovules in all examined ovules in transgenic lines. Scale bars, 25 µm. **e**, Corrected total cell fluorescence (CTCF) of LM19 immunosignals in the nucellus of WT, *mads31* and *Ubi::NRPD4b* ovules at Ov10 stage. The data are shown as mean ± s.d.; $n = 5, 5, 9, 7, 9$ ovules for each genotype; *t*-test for unpaired two-sample data, two-sided.

https://doi.org/10.1038/s41477-025-01915-z

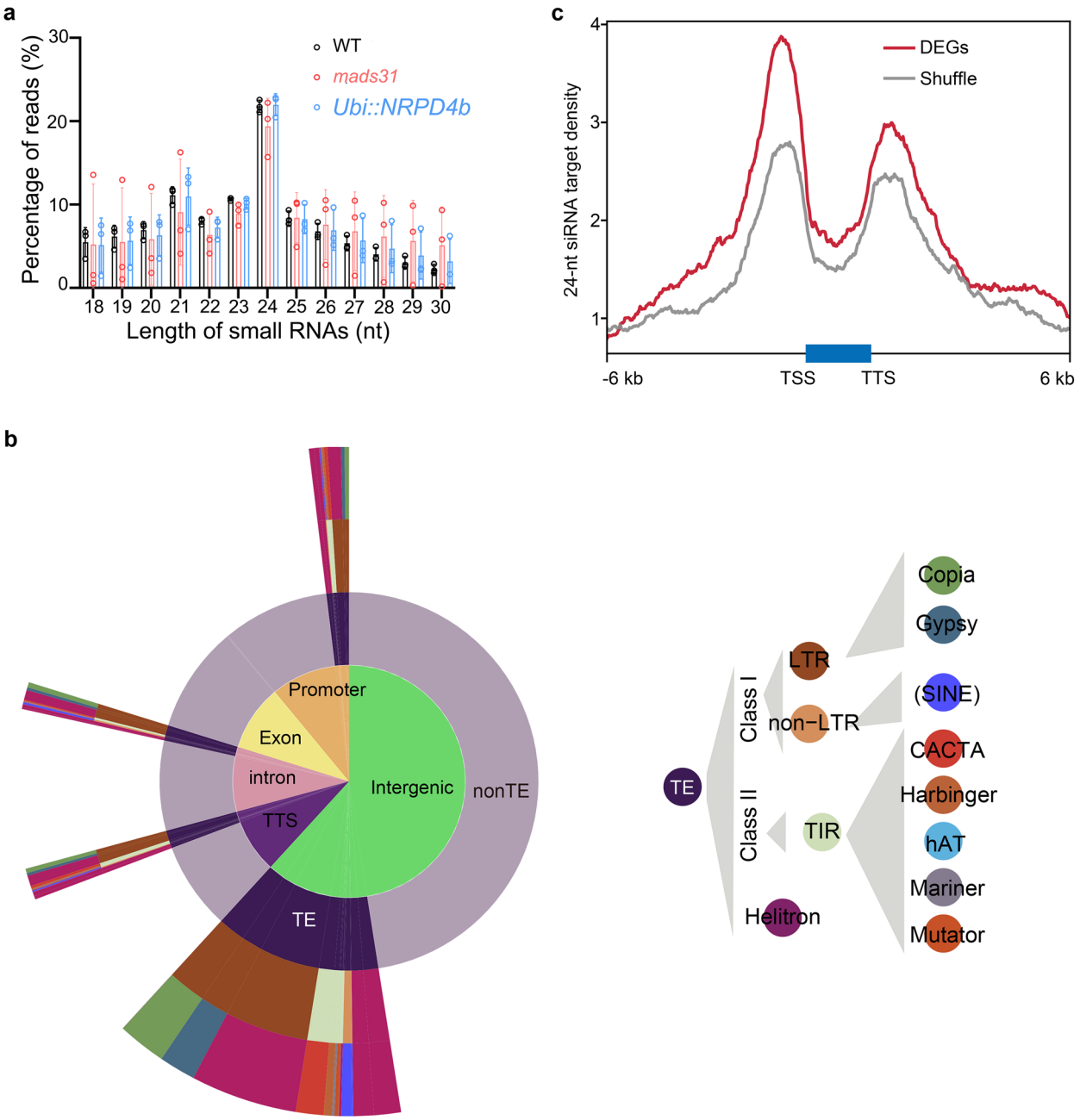

Extended Data Fig. 9 | Summary of small RNA sequencing. a, Size distribution of sRNAs in WT, *mads31* and *Ubi::NRPD4b* pistils. The data are shown as mean ± s.d.; n = 3 replicates for each genotype. **b**, Left, circle plots showing the distribution of 24-nt siRNA recognition sites in the barley genome (inner circle) and the proportion of target transposable elements (outer circle); right, annotation of TE type and superfamily. Colours indicate the different TE types. **c**, Metaplot showing the enrichment of target density of 24-nt siRNA within a 12 kb interval of DEGs, in comparison with random unchanged genes. TSS, transcription start site, TTS, transcription termination site.

https://doi.org/10.1038/s41477-025-01915-z

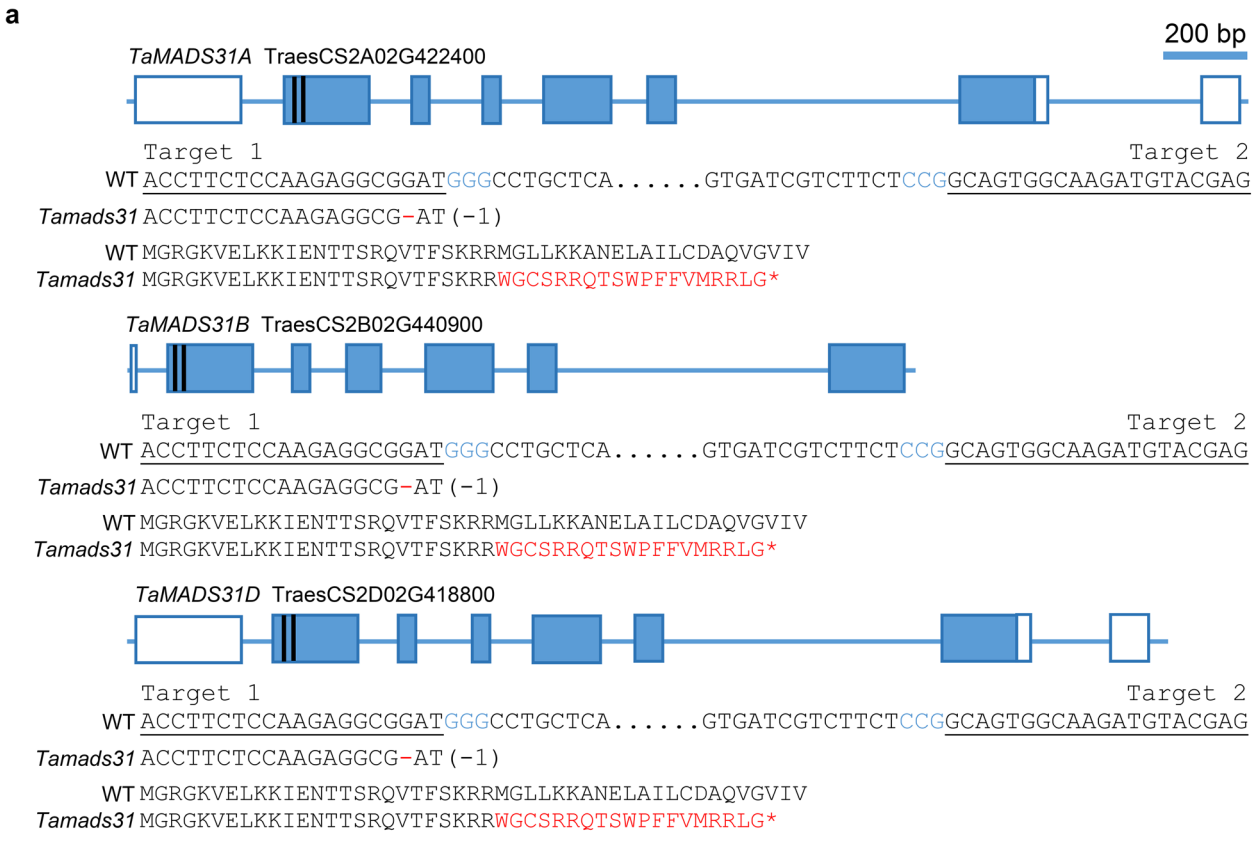

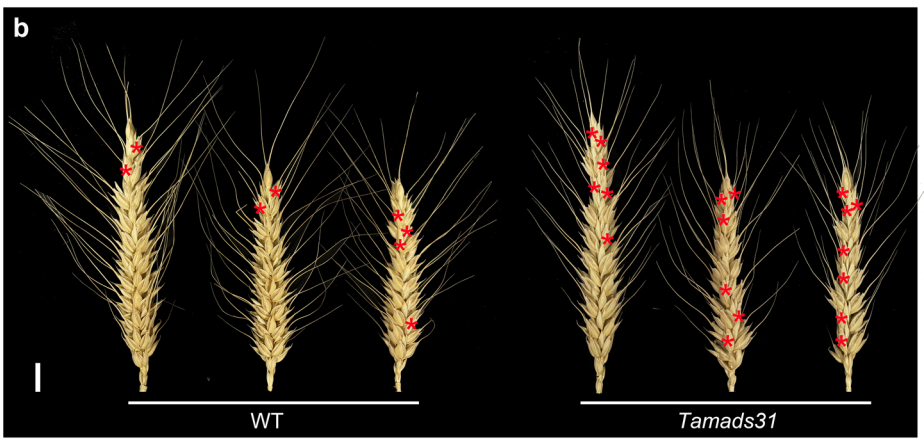

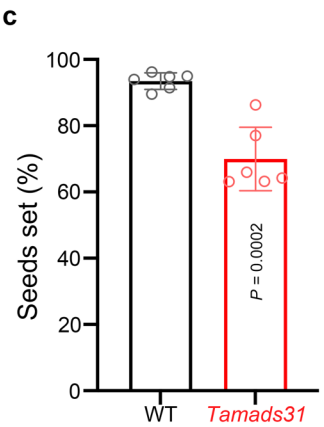

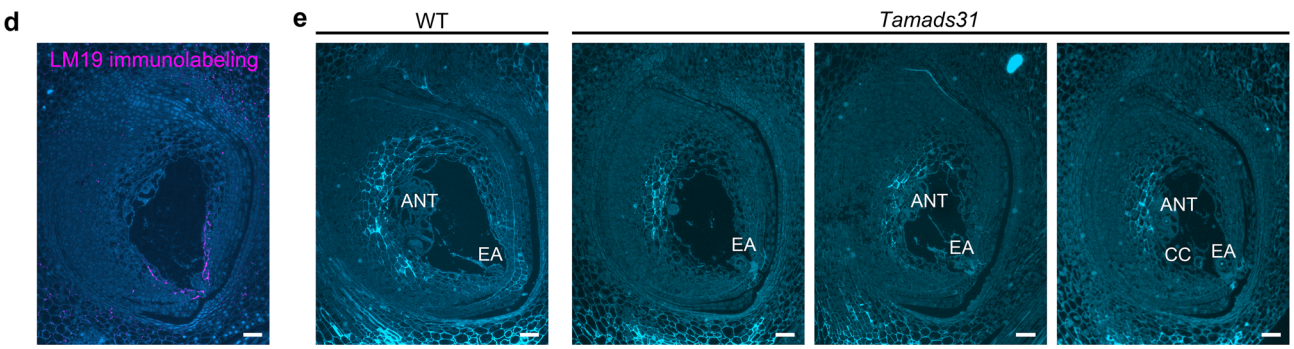

Extended Data Fig. 10 | Creation of a wheat *Tamads31* mutant using CRISPR/Cas9. a, Upper, the gene structure of each copy of *TaMADS31* and the positions of two sgRNA targets (black lines) for gene editing. Blue boxes are exons and white boxes are UTRs. Middle, DNA sequence of the mutation in *TaMADS31A/B/D*. Lower, putative amino acid sequences in the *Tamads31* mutant. Asterisks indicate a stop codon. WT, wild type. **b**, Mature spikes of WT and *Tamads31*. Red asterisks indicate sterile florets. Scale bar, 1 cm. **c**, Seed setting rate of WT and *Tamads31*. The data are shown as mean ± s.d.; $n = 6$ plants, t-test, two-sided. **d**, LM19 immunolabeling in a wheat ovule at stage Ov10. **e**, Calcofluor White stained longitudinal sections of WT and *Tamads31* ovules at Ov10 stage. ANT, antipodal cells; CC, central cell; EA, egg apparatus. Scale bars, 50 µm. Representative images were shown from sections of 5 ovules for each stage and each genotype.

nature portfolio

Corresponding author(s): Matthew Tucker

Last updated by author(s): Nov 25, 2024

Reporting Summary

Nature Portfolio wishes to improve the reproducibility of the work that we publish. This form provides structure for consistency and transparency in reporting. For further information on Nature Portfolio policies, see our Editorial Policies and the Editorial Policy Checklist.

Statistics

For all statistical analyses, confirm that the following items are present in the figure legend, table legend, main text, or Methods section.

n/a	Confirmed	
☐	☒	The exact sample size (*n*) for each experimental group/condition, given as a discrete number and unit of measurement
☐	☒	A statement on whether measurements were taken from distinct samples or whether the same sample was measured repeatedly
☐	☒	The statistical test(s) used AND whether they are one- or two-sided *Only common tests should be described solely by name; describe more complex techniques in the Methods section.*
☒	☐	A description of all covariates tested
☐	☒	A description of any assumptions or corrections, such as tests of normality and adjustment for multiple comparisons
☐	☒	A full description of the statistical parameters including central tendency (e.g. means) or other basic estimates (e.g. regression coefficient) AND variation (e.g. standard deviation) or associated estimates of uncertainty (e.g. confidence intervals)
☐	☒	For null hypothesis testing, the test statistic (e.g. *F*, *t*, *r*) with confidence intervals, effect sizes, degrees of freedom and *P* value noted *Give P values as exact values whenever suitable.*
☒	☐	For Bayesian analysis, information on the choice of priors and Markov chain Monte Carlo settings
☒	☐	For hierarchical and complex designs, identification of the appropriate level for tests and full reporting of outcomes
☒	☐	Estimates of effect sizes (e.g. Cohen's *d*, Pearson's *r*), indicating how they were calculated

Our web collection on statistics for biologists contains articles on many of the points above.

Software and code

Policy information about availability of computer code

Data collection

Images of in situ hybridization and resin section were collected using NIS-Elements AR (Nikon, version v4.2) and ZEN blue edition (Zeiss, v3.5);
Image if DNA gel was collected by Image Lab (Bio-Rad,v5.2);
Images of LM19 immunolabelling were collected using ZEN blue edition (Zeiss, v3.5);
Confocal images were collected with NIS-Elements AR (Nikon, v4.30.01);
Dual-LUC data were collected with GloMax®-96 Microplate Luminometer (Promega, v1.9.3).

Data analysis	qRT-PCR and ChIP-PCR assays were analyzed with QuantStudio (Thermo Fisher, v1.3). ImageJ (v1.53a) was used for fluorescence signal quantification. Tissue areas were measured using ZEN blue edition (Zeiss, v3.5). For RNA-seq: Raw reads were examined using FastQC (version 0.11.4), and were filtered by Trimmomatic (version 0.38) with default parameter. Then filtered reads were aligned to the barley Morex V1 genome (http://webblast.ipk-gatersleben.de) using HISAT2 (version 2.0.0) program. Read counts per kilobase per million (RPKM) was normalised using HTSeq (version 0.11.2, https://htseq.readthedocs.io/en/master/).The differential expressed genes were analyzed by DESeq2 (version 3.11). DEGs were further annotated by BLASTX (v2.10) against protein databases of Arabidopsis (https://www.arabidopsis.org) and rice (http://rice.uga.edu). Gene ontology enrichment was analyzed by R package 'clusterProfiler' (v3.11). The expression heatmap was created using ClustVis 2.0. For small RNA-seq:Raw reads were filtered by removing low quality reads and adapter containing reads using fastp (v0.24.0). Clean reads were mapped to the barley genome (MorexV3_pseudomolecules_assembly) using Bowtie (version 1.0.1). 24nt siRNA targets were filtered out based on mapped fragments length, and the 24nt siRNA targets were annotated by using HOMER (http://homer.ucsd.edu/homer/ngs/customGenomes/index.html)(v4.4). In 24nt siRNA targets density analysis, the 24nt siRNA targets number was calculated based on 1kb genome bins through BEDTools (v2.31.0). Graphpad Prism 9 and Microsoft Excel 2016 was used for statistical analysis and graphs data presentation.

For manuscripts utilizing custom algorithms or software that are central to the research but not yet described in published literature, software must be made available to editors and reviewers. We strongly encourage code deposition in a community repository (e.g. GitHub). See the Nature Portfolio guidelines for submitting code & software for further information.

Data

Policy information about availability of data

All manuscripts must include a data availability statement. This statement should provide the following information, where applicable:

- Accession codes, unique identifiers, or web links for publicly available datasets
- A description of any restrictions on data availability
- For clinical datasets or third party data, please ensure that the statement adheres to our policy

All data generated or analyzed during this study were included in this published article and supplementary files. Bio-reagents are available for research propose upon request from the corresponding author under a material transfer agreement.

Research involving human participants, their data, or biological material

Policy information about studies with human participants or human data. See also policy information about sex, gender (identity/presentation), and sexual orientation and race, ethnicity and racism.

Reporting on sex and gender	N/A
Reporting on race, ethnicity, or other socially relevant groupings	N/A
Population characteristics	N/A
Recruitment	N/A
Ethics oversight	N/A

Note that full information on the approval of the study protocol must also be provided in the manuscript.

Field-specific reporting

Please select the one below that is the best fit for your research. If you are not sure, read the appropriate sections before making your selection.

☒ Life sciences ☐ Behavioural & social sciences ☐ Ecological, evolutionary & environmental sciences

For a reference copy of the document with all sections, see nature.com/documents/nr-reporting-summary-flat.pdf

Life sciences study design

All studies must disclose on these points even when the disclosure is negative.

Sample size	The barley ovule is the female reproductive organ, located within the pistil and surrounded by stamens and other floral structures. To examine the inner structure and cell morphology of barley ovules, thin sectioning is the most effective method. This technique requires precise sample orientation to obtain 2-5 longitudinal sections from the central region of the ovule, which contains the female germline. As a result, obtaining a large number of samples is challenging. To minimize bias, 50-100 spikelets or pistils were collected from each developmental stage and genotype. A certain number of spikelets or pistils were randomly picked for various experiments. Sample sizes are indicated in the figures, legends and main text.
Data exclusions	No data were excluded from the analysis.

Replication	All experimental findings were reproduced in several independent biological experiments (n) with multiple technical replicates. The number of repeats is indicated in the figures and figure legends. Main Conclusions were confirmed in different plant genetic backgrounds and multiple temperature treatments. All attempts to replicate the experiments were successful and approved by multiple researchers.
Randomization	All plants materials use in this study were grown in environment-controlled chambers. Pots positions were randomly arranged. Samples od each genotype were randomly collected from multiple tillers of 1-6 plants and pooled for downstream experiments.
Blinding	Investigators were not blinded to plant genotypes during experiments. The research materials are plants so the blinding design is not applicable to this system. Experiment results are not subjective.

Reporting for specific materials, systems and methods

We require information from authors about some types of materials, experimental systems and methods used in many studies. Here, indicate whether each material, system or method listed is relevant to your study. If you are not sure if a list item applies to your research, read the appropriate section before selecting a response.

Materials & experimental systems

n/a	Involved in the study
☐	☒ Antibodies
☒	☐ Eukaryotic cell lines
☒	☐ Palaeontology and archaeology
☒	☐ Animals and other organisms
☒	☐ Clinical data
☒	☐ Dual use research of concern
☐	☒ Plants

Methods

n/a	Involved in the study
☒	☐ ChIP-seq
☒	☐ Flow cytometry
☒	☐ MRI-based neuroimaging

Antibodies

Antibodies used	Mouse anti GFP-Tag mAb (AB Clonal Biotechnology, Cat No. AE012, dilution 1:300); Rat IgM monoclonal antibody anti-de-methyl-esterified homogalacturonan LM19 (PlantProbes, Cat No. ELD001, 1:100 dilution); Mouse monoclonal H3 di methyl K9 antibody anti-H3K9me2 (Abcam, Cat No. ab1220, 1:400 dilution); Rabbit IgG polyclonal antibody anti-H3K27me1 (ThermoFisher Scientific, Cat No. 49-1012, 1: 600 dilution); Goat anti-Rat IgG (H+L) Highly Cross-Adsorbed Secondary Antibody, Alexa Fluor™ Plus 555 (Invitrogen, Cat No. A48263, 1:200 dilution); Goat anti-Rabbit IgG (H+L) Highly Cross-Adsorbed Secondary Antibody, Alexa Fluor™ Plus 488 (Invitrogen, Cat No. A32731, 1:400 dilution); Goat anti-Mouse IgG (H+L) Cross-Adsorbed Secondary Antibody, Alexa Fluor™ 488 (Invitrogen, Cat No. A-11001, 1:400 dilution); anti-DIG-AP (Roche, Cat No. 11093274910; 1: 1,000 dilution).
Validation	1. The commercial anti-GFP has been well validated for Immunoprecipitation in the several published papers and in our manuscript (Fig. 5). Product profile: https://abclonal.com/catalog-antibodies/MouseantiGFPTagmAb/AE012 2. The commercial anti-pectin has been validated in several plant cell wall researches an in our study (Figs 2 and 5). Product profile: https://www.kerafast.com/item/1583/anti-pectic-polysaccharide-homogalacturonan-lm19-antibody 3. The commercial anti-H3K9me2 has been validated in plants and our study (Fig 6). Product profile: https://www.abcam.com/products/primary-antibodies/histone-h3-di-methyl-k9-antibody-mabcam-1220-chip-grade-ab1220.html 4. The commercial anti-H3K27me1 has been validated in plants and our study (Fig 6). Product profile: https://www.thermofisher.com/antibody/product/H3K27me1-Antibody-Polyclonal/49-1012 5. The commercial secondary antibodies (anti-rat/rabbit/mouse IgG) have been well validated in numerous researches. 6. The commercial anti-Digoxigenin-AP, Fab fragments, has been well validated for In situ mRNA hybridisation in the several published papers and in our study (Figs. land 5), and the antibody profile can be found in the following link: https://www.sigmaaldrich.com/catalog/product/roche/11093274910?lang=en&region=AU

Dual use research of concern

Policy information about dual use research of concern

Hazards

Could the accidental, deliberate or reckless misuse of agents or technologies generated in the work, or the application of information presented in the manuscript, pose a threat to:

No	Yes	
☒	☐	Public health
☒	☐	National security
☒	☐	Crops and/or livestock
☒	☐	Ecosystems
☒	☐	Any other significant area

Experiments of concern

Does the work involve any of these experiments of concern:

No	Yes	
☒	☐	Demonstrate how to render a vaccine ineffective
☒	☐	Confer resistance to therapeutically useful antibiotics or antiviral agents
☒	☐	Enhance the virulence of a pathogen or render a nonpathogen virulent
☒	☐	Increase transmissibility of a pathogen
☒	☐	Alter the host range of a pathogen
☒	☐	Enable evasion of diagnostic/detection modalities
☒	☐	Enable the weaponization of a biological agent or toxin
☒	☐	Any other potentially harmful combination of experiments and agents

Plants

Seed stocks	Wild type barley cultivar 'Golden Promise' and wild type wheat cultivar 'Fielder' are obtained at Waite Research Institute, Urrbrae, South Australia, Australia.
Novel plant genotypes	1. mads31 mutants: barley mutants were generated by an optimized CRISPR/Cas9 gene editing system (Ma et al., 2015). Two targets were designed to cause mutation approaching the start codon (target 1 GTCGGGGTGATCGTCTTCTCCGG; target 2 ACCTTCTCCAAGAGGCGGATGGG). SgRNA–target 1 (T1) was driven by rice promoter OsU6c, and sgRNA–T2 was driven by rice promoter OsU3. The sgRNA expression cassettes of OsU6c–sgRNA–T1 and OsU3–sgRNA–T2 were amplified from pYLsgRNA–OsU6c and pYLsgRNA–OsU3 plasmids using Phusion High-Fidelity DNA Polymerase (New England BioLabs) and cloned into a binary vector, pYLCRISPR–Cas9PUbi–H, using two BsaI sites. The whole vector carrying Cas9 and sgRNA expression cassettes was transformed into immature embryos of Golden Promise using an A. tumefaciens AGL1-mediated transformation method. Wheat mutant was also generated by a modified CRISPR/Cas9 system. Two target sequences (T1 and T2) for sgRNA were selected to edit all three homologues of the TaMADS31 gene. TaU3-sgRNA-T1 and TaU6-sgRNA-T2 expression cassettes were cloned into a binary vector pBUE411 and the vector was transformed into immature embryos of Fielder using an A. tumefaciens EHA105-mediated method. Mutations were identified by Sanger sequencing (AGRF) of the targets and flanking region. 2. Pro::MADS31-eGFP in WT and in mads31 background: a ~4kb genomic DNA fragment including 2.4kb of promoter and the full genomic coding region of MADS31 were fused in frame to eGFP and inserted between the HindIII and BstEII sites of pCAMBIA1301, which was next transformed in to Golden Promise. Over 10 lines were generated in T0. Three lines and their offspring generations (T1-T4) were used for the study. For ChIP, a mixture of samples from all lines was collected as a sample pool. 3. Ubi::MADS31: the full length MADS31 coding sequences was inserted into vector pU1301, which was next transformed into Golden Promise. No seeds were obtained from two T0 plants because of extremely retarded growth. 4: Ubi::NRPD4b: the full length NRPD4b coding sequences was inserted into vector pU1301, which was next transformed into Golden Promise. Seven T0 lines were used for expression level examination. Three T0 lines were used for detailed phenotyping and LM19-immuno-labeling and their T2 offspring were used for small RNA sequencing and histone H3 methylation immunolabeling.
Authentication	1. mads31 mutants: mutations were identified by Sanger sequencing two generations of plants. Plants carrying Cas9 were determined by PCR and discarded to prevent residue editing activities. A stable phenotype was observed from up to six generations of mutants in the environment-controlled growth chamber. 2. Pro::MADS31-eGFP in WT and mads31: ovules of Ov8-Ov10 stages were dissected from spikelets of transgenic plants and examined under a fluorescence microscope. The lines showing GFP signals were kept and used for study. 3. Ubi::MADS31: PCR of inserted fragment in the construct was used to determine genotype. 4: Ubi::NRPD4b: PCR of the inserted fragment in the construct was used to determine genotype, and 'partial fertility phenotype was used as a supportive screening method.